Functional contributions of HCN channels in the primary auditory neurons of the mouse inner ear

Functional contributions of HCN channels in the primary auditory neurons of the mouse inner ear

Ye-Hyun Kim[1,2] and Jeffrey R. Holt[2]

[1]Neuroscience Graduate Program, University of Virginia School of Medicine, Charlottesville, VA 22908
[2]Department of Otolaryngology, F.M. Kirby Neurobiology Center, Boston Children's Hospital and Harvard Medical School, Boston, MA 02115

The hyperpolarization-activated current, I_h, is carried by members of the *Hcn* channel family and contributes to resting potential and firing properties in excitable cells of various systems, including the auditory system. I_h has been identified in spiral ganglion neurons (SGNs); however, its molecular correlates and their functional contributions have not been well characterized. To investigate the molecular composition of the channels that carry I_h in SGNs, we examined *Hcn* mRNA harvested from spiral ganglia of neonatal and adult mice using quantitative RT-PCR. The data indicate expression of *Hcn1*, *Hcn2*, and *Hcn4* subunits in SGNs, with *Hcn1* being the most highly expressed at both stages. To investigate the functional contributions of HCN subunits, we used the whole-cell, tight-seal technique to record from wild-type SGNs and those deficient in *Hcn1*, *Hcn2*, or both. We found that HCN1 is the most prominent subunit contributing to I_h in SGNs. Deletion of *Hcn1* resulted in reduced conductance (G_h), slower activation kinetics (τ_{fast}), and hyperpolarized half-activation ($V_{1/2}$) potentials. We demonstrate that I_h contributes to SGN function with depolarized resting potentials, depolarized sag and rebound potentials, accelerated rebound spikes after hyperpolarization, and minimized jitter in spike latency for small depolarizing stimuli. Auditory brainstem responses of *Hcn1*-deficient mice showed longer latencies, suggesting that HCN1-mediated I_h is critical for synchronized spike timing in SGNs. Together, our data indicate that I_h contributes to SGN membrane properties and plays a role in temporal aspects of signal transmission between the cochlea and the brain, which are critical for normal auditory function.

The Journal of General Physiology

INTRODUCTION

Spiral ganglion neurons (SGNs) are the first-order sensory neurons of the auditory system, which provide afferent innervation of hair cells in the mammalian cochlea. SGNs convey signals from hair cells to the brain in a manner that preserves the amplitude, frequency, and temporal aspects of sound information (Geisler, 1998; Taberner and Liberman, 2005; Meyer and Moser, 2010). This high-fidelity signal transmission between the hair cells and the SGNs is critical for normal auditory processing and sound localization.

To perform these functions, SGNs express a variety of voltage-gated ion channels that allow efficient signal transfer from inner hair cells (IHCs; Davis, 2003). The expression of specific voltage-gated ion channels in SGNs allows them the ability to precisely encode graded membrane potentials of hair cells into trains of action potentials (APs). For example, SGNs express voltage-gated calcium and potassium channels along the cochlear tonotopic axis in a graded manner that reflects the tonotopic specialization of hair cells (Adamson et al., 2002; Davis, 2003; Chen et al., 2011; Lv et al., 2012).

The hyperpolarization-activated cationic current, I_h, has been identified in neurons of the auditory system (Banks et al., 1993; Bal and Oertel, 2000; Koch and Grothe, 2003), including SGNs (Chen, 1997; Mo and Davis, 1997; Yi et al., 2010), but the molecular composition of the channels that carry I_h and their precise function have not been clarified. I_h is carried by subunits of the HCN channel family, HCN1–4, which form homo- and heterotetrameric channels (Ludwig et al., 1998; Ishii et al., 1999). Unlike other channels that activate upon depolarization, I_h activates in response to membrane hyperpolarization negative to −50 mV and passes inward current that depolarizes the cell membrane. Thus, the unusual biophysical properties of I_h contribute to resting membrane potential and firing properties in many different cell types (Robinson and Siegelbaum, 2003; Biel et al., 2009).

Recently, Yi et al. (2010) characterized I_h at the hair cell afferent synapse; however, the molecular correlates of I_h and their functional contributions in SGN cell bodies were not examined. To identify which *Hcn* genes are expressed in neonatal and adult SGNs, we harvested

Correspondence to Jeffrey R. Holt: Jeffrey.Holt@Childrens.Harvard.edu

Abbreviations used in this paper: ABR, auditory brainstem response; AP, action potential; CI, confidence interval; IHC, inner hair cell; qPCR, quantitative RT-PCR; SGN, spiral ganglion neuron.

The Rockefeller University Press $30.00
J. Gen. Physiol. Vol. 142 No. 3 207–223
www.jgp.org/cgi/doi/10.1085/jgp.201311019

SGN mRNA for quantitative RT-PCR (qPCR) analysis. To examine the contributions of *Hcn* gene expression to I_h, we recorded from SGNs of WT mice and mice that lacked *Hcn1*, *Hcn2*, or both. Our qPCR and electrophysiology data indicate expression of HCN1, HCN2, and HCN4 subunits in SGNs, with HCN1 being the most highly expressed subunit. Deletion of *Hcn1* resulted in reduced conductance, hyperpolarized half-activation voltage, and slower activation kinetics. We recorded from SGNs in current-clamp mode to investigate the functional contributions of I_h to SGN membrane and firing properties. We show that I_h depolarizes SGN resting membrane potentials, regulates rebound spike timing, and synchronizes AP firing in response to small depolarizing stimuli. In addition, auditory brainstem responses (ABRs) indicate possible auditory deficits in $Hcn1^{-/-}$ animals. $Hcn1^{-/-}$ mice had delayed ABR latencies, suggesting a contribution to spike timing in the eighth cranial nerve. Collectively, the present study provides evidence that I_h, HCN1 in particular, contributes to the membrane properties of SGNs and plays a role in the temporal aspects of auditory signal transmission required for normal auditory function.

MATERIALS AND METHODS

Animals

All animal protocols used in this study were approved by the Institutional Animal Use and Care Committee at the University of Virginia (protocol #3123) and Boston Children's Hospital (protocol #11-04-1959). Experiments were performed in strict accordance to the guidelines therein. *Hcn1*-deficient ($Hcn1^{-/-}$) mice (strain: B6.129S-$Hcn1^{tm2Kndl}$/J; Nolan et al., 2003) were obtained from The Jackson Laboratory, and *Hcn2*-deficient ($Hcn2^{-/-}$) mice were obtained originally from A. Ludwig (Friedrich-Alexander-Universität Erlangen-Nürnburg, Erlangen, Germany; Ludwig et al., 2003). Mice deficient in *Hcn1* and *Hcn2* ($Hcn1/2^{-/-}$) mice were generated by crossing $Hcn1^{+/-}$ and $Hcn2^{+/-}$ mice, as previously described (Horwitz et al., 2011). Both sexes of animals were used in nondiscriminatory fashion. WT control data were obtained from three different strains, Swiss Webster (Charles River; n = 11 SGNs), WT littermates (n = 5) obtained from $Hcn1^{+/-}$ and $Hcn1^{+/-}$ crosses, and WT littermates (n = 9) obtained from $Hcn2^{+/-}$ and $Hcn2^{+/-}$ crosses. We found no statistical difference in any of the analyzed parameters and have pooled the WT data.

Neonatal SGN preparation

SGNs were acutely dissected from neonatal mice, age ranging between postnatal day (P) 1 and P8. After rapid decapitation, cochleae from both sides of the inner ear were excised from the temporal bone and bathed in sterile MEM with GlutaMAX (Gibco) supplemented with 10 mM HEPES (Sigma-Aldrich) and 25 mg ampicillin (Sigma-Aldrich), pH 7.4. The bony labyrinth encapsulating the cochlea was chipped away to gain access to the whole cochlear turn, and the spiral ligament and stria vascularies were peeled off. SGNs were isolated carefully from the cochlear modiolus by severing the central fiber tracts that connect to the cochlear nucleus. No enzyme was used for SGN dissection. Care was given so that the SGN peripheral fibers and the organ of Corti were left relatively intact. SGN explants were divided into halves as base and apex in relation to the cochlear tonotopic axis and mounted flat on glass coverslips (Thermo Fisher Scientific), with organ of Corti facing down to gain better access to SGN cell bodies. The sections were secured in place under two thin glass fibers glued to the coverslip with Sylgard 184 (Dow Corning). SGN organotypic explants were incubated at 37°C in a humidified incubator (5% CO_2) for 1–2 h, after which they were used for acute electrophysiological experiments. All SGN explants were used within 4–5 h after dissection.

Type I SGNs

SGNs can be categorized into type I and type II neurons based on their innervation pattern and morphology. Type I neurons, which constitute 90–95% of the entire SGN population, innervate IHCs and are responsible for sound information transfer (Liberman, 1982). Type I neurons are highly myelinated (Romand and Romand, 1987) and in general have relatively large cell body size compared with type II neurons (Rusznák and Szűcs, 2009). The myelin sheath tightly covers the axon fibers and loosely wraps around the cell bodies of SGNs, ensuring high velocity signal conduction to the central pathway. In contrast, type II neurons, which compose the remaining ∼5% of SGNs, innervate the outer hair cells (Perkins and Morest, 1975). Type II neurons are unmyelinated and have smaller cell bodies than type I neurons (Rusznák and Szűcs, 2009). The different morphology and abundance in number allowed for easy detection of neonatal type I SGNs for electrophysiological recordings. All neonatal SGN data presented in this paper were obtained from type I cells.

Adult SGN culture

Adult mouse SGN culture technique was performed in accordance to the method previously described (Lv et al., 2010). Adult mouse was sacrificed and decapitated rapidly. For each culture, three to four animals were pooled. Temporal bones were removed from the skull and bathed in ice-cold MEM with Hank's salt (Gibco) supplemented with 0.2 mg/ml kynurenic acid (Sigma-Aldrich), 10 mM $MgCl_2$, 2% (vol/vol) FBS (Gibco), and 6 g/liter D-glucose (Sigma-Aldrich). The bony shell encapsulating the cochlea was chipped off using a scalpel, and the organ of Corti was removed from the central core. The modiolus, which contained the SGNs, was isolated in the above dissecting media, in which the 2% (vol/vol) FBS was replaced with 2% (vol/vol) B27 (Gibco), and split into apical and basal sections. The sections were subsequently digested in enzyme solution containing 1 mg/ml collagenase type 1 (Sigma-Aldrich) and 1 mg/ml DNase (Sigma-Aldrich) at 37°C for 15 min. After enzyme treatment, 0.25% trypsin (Gibco) was added to the solution and incubated for an additional 10 min at 37°C. The reaction was quenched with equal volume FBS (vol/vol). After gentle trituration, the cell solution was transferred to Hank's balanced salt solution (HBSS) containing 0.45 M sucrose (Sigma-Aldrich) and centrifuged at 2,000 rpm for 5 min. The cell pellets were reconstituted in Neurobasal A (Gibco) supplemented with 2% B27, 0.5 mM L-glutamine (Sigma-Aldrich), and 100 U/ml penicillin (Sigma-Aldrich). The freshly isolated SGN cells were filtered through a 40-µm cell strainer and plated onto glass coverslips, pretreated with 0.5 mg/ml poly-D-lysine (Sigma-Aldrich) and 1 mg/ml laminin (Sigma-Aldrich). The SGN culture was supplied with 10% FBS, 0.2 mg/ml kynurenic acid, 10 ng/µl NT3 (Sigma-Aldrich), and 10 ng/µl BDNF (Sigma-Aldrich) and incubated at 37°C in a humidified incubator (5% CO_2) for 24–48 h before electrophysiological recordings. To ensure quality recording and minimize space-clamp errors, only spherical SGNs with one or two neurites were selected for voltage-clamp recordings.

Electrophysiology

The whole-cell, tight-seal patch clamp technique was used in voltage- and current-clamp modes to record I_h from SGN cell bodies. All electrophysiological recordings were performed at

room temperature (22–24°C). SGN explants were placed into a custom-made recording chamber and viewed under an Axioskop FS upright microscope (Carl Zeiss) equipped with 63× water-immersion lens and differential interface contrast optics. SGN explants were bathed in a standard external solution that contained (mM): 137 NaCl, 0.7 NaH_2PO_4, 5.8 KCl, 1.3 $CaCl_2$, 0.9 $MgCl_2$, 5.6 D-glucose, 10 HEPES, amino acids (1:50; Gibco), and vitamins (1:100; Gibco). The pH was adjusted to 7.4 with NaOH and the measured osmolarity was 303 mOsmol/kg. Recording pipettes (3–5 MΩ) were pulled from R-6 soda lime capillaries (King Precision Glass) using a two-stage vertical pipette puller (PC-10; Narishige). To minimize pipette capacitance, tips were coated with ski wax. Recording pipettes were filled with standard internal solution that contained (mM): 135 KCl, 2.5 $MgCl_2$, 2.5 K_2-ATP, 5.0 HEPES, 5.0 EGTA, and 0.1 $CaCl_2$, pH 7.4 (KOH), 283 mOsmol/kg. All reagents for electrophysiology solution were purchased from Sigma-Aldrich, unless otherwise noted. I_h was recorded immediately after the cell membrane was broken through at gigaohm (GΩ) seal. Series resistance (R_s) and membrane capacitance (C_m) were corrected. Both parameters were continuously monitored to ensure stable recording. Compensated residual R_s was <7 MΩ on average.

For pharmacology experiments, the following drugs were applied to the external bath: 100 µM ZD7288 (Tocris Bioscience), 100 µM Ni_2Cl (Sigma-Aldrich), and 200 µM 8-br-cAMP (Sigma-Aldrich). Chemicals were dissolved in deionized water (dH_2O) to appropriate stock concentrations, stored at −20°C, and applied directly to the external solution at the desired final concentrations.

Electrophysiological data from SGNs was recorded using an Axopatch200B (Molecular Devices) amplifier. Signals were filtered at 1 kHz with a low pass Bessel filter and digitized at ≥20 kHz using 12-bit acquisition system, Digidata 1332 (Axon Instruments), and pClamp 9.0 (Molecular Devices). All stimulus protocols were generated using pClamp 9.0, and data were stored on a PC.

SGN microdissection and qPCR

Neonatal SGN tissue was harvested from P3 Swiss Webster mice in ice-cold MEM with GlutaMAX, supplemented with 10 mM HEPES (Sigma-Aldrich) and 25 mg ampicillin (Sigma-Aldrich), pH 7.4. SGNs were gently isolated from cochlear modiolus by severing the central processes. To prevent cross-contamination from cochlear hair cells, organ of Corti was trimmed away along the cochlear turn using a microblade so that the SGN isolates only contained cell bodies. Microdissected SGNs were rinsed in fresh MEM, transferred into microcentrifuge tubes, and rapidly frozen on dry ice. Two preparations of SGN tissue were pooled from 10 (five mice) and 14 (seven mice) cochleas, respectively, and were processed in parallel for RNA isolation and qPCR experiments.

Adult SGNs were harvested from Swiss Webster mice ≥P40. Temporal bones were removed from the skull and bathed in ice-cold MEM with Hank's salt supplemented with 0.2 mg/ml kynurenic acid. The bony shell encapsulating the cochlea was chipped away using a scalpel. SGNs were excised from the central core, and processes were sectioned where the cochlear nerve joins the vestibular nerve to prevent contamination from vestibular neurons. Dissected SGN tissue was rapidly frozen in dry ice. Two samples of adult SGN tissue were pooled from 6 (three mice) and 10 (five mice) cochleas, respectively, and were processed in parallel for RNA isolation and subsequent qPCR experiments.

The frozen SGN microisolates were thawed, spun down in a centrifuge to remove excess media, and processed for RNA isolation. Total SGN RNA was prepared with an RNAqueous micro kit (Ambion) according to the manufacturer's instruction. The isolated RNA was then purified with a DNA-free RNA kit (Zymo Research) and stored in −80°C. RNA concentration was measured on a spectrophotometer (Nanodrop ND-1000; Thermo Fisher Scientific). For RNA quality control, the samples were analyzed with a Bioanalyzer (Agilent Technologies) and found to have an RNA integrity number of >9.0. 100 ng RNA was reverse transcribed into cDNA using the QuantiTect Reverse Transcription kit (QIAGEN). qPCR was performed in triplicates using SYBR Green ER qPCR Supermix (Invitrogen) according to the manufacturer's instructions and processed on a CFx Real-Time PCR Detection System (Bio-Rad Laboratories). Each reaction (25 µl) included primers at 0.2–0.4 pM and cDNA generated from 5 ng RNA. qPCR parameters were set for 40 cycles, and amplicon purity was confirmed with melt curve analysis. qPCR primers had melting temperatures ranging from 58 to 61°C, and the sequences were as follows: *Hcn1*, 5′-ACATGCTGTGCATTGGTTATGGCG-3′ and 5′-AACAAACATTGCGTAGCAGGTGGC-3′; *Hcn2*, 5′-ACTTCCGCACCGGCATTGTTATTG-3′ and 5′-TCGATTCCCTTCTCCACTATGAGG-3′; *Hcn3*, 5′-CCTCATCCGCTACATACACCAGT-3′ and 5′-GACACAGCAGCAACATCATTCC-3′; and *Hcn4*, 5′-ACTTTAACTGCCGAAAGCTGGTGG-3′ and 5′-GAAACGCAACTTGGTCAGCATGGA-3′. qPCR primer sets were designed to amplify specific regions of HCN amplicons produced by RT- PCR (Horwitz et al., 2010).

Expression levels and possible genomic DNA contamination were tested with ribosomal 29S as housekeeping gene by running reverse transcribed cDNA samples and no-reverse transcript controls simultaneously. Cochlear hair cell contamination was determined with cochlear hair cell–specific gene *prestin* as a control. The sequences of ribosomal 29S and *prestin* primers (Lelli et al., 2009) were as follows: *29S*, 5′-GGAGTCACCCACGGAAGTTCG-3′ and 5′-GGAAGCACTGGCGGCACATG-3′; and *prestin*, 5′-TTACGGCTCGATTTGGAGGGTGAA-3′ and 5′-GTGCAAGAGGCCTGTTAATCTTTG-3′.

ABRs

Hcn1$^{-/-}$ mice ($n = 7$) and their WT littermates ($n = 5$) were used for the ABR recording. Because of the mixed genetic background (C57BL/6 and 129S) of the strain, mice were tested at 6–7 wk of age to minimize confounding factors from age-related hearing loss that these strains exhibit around 3 mo of age (Zheng et al., 1999; Kane et al., 2012).

ABRs were performed in a sound-proof chamber. Before ABR measurements, mice were anesthetized with 100 mg/kg ketamine and 20 mg/kg xylazine via intraperitoneal injection and placed on a heating pad to maintain body temperature. Needle electrodes were placed subdermally at the vertex and below the pinna, and a ground electrode was placed near the tail. Tone pips (5 ms, 40 Hz) at varying frequencies (5.6, 8, 11.3, 16, 22.6, and 32 kHz) were delivered to the right ear via a sound system, in which dual sound source was coupled to a microphone and positioned near the ear canal. Each stimulus was presented with alternating polarities, and the responses were recorded with increasing sound pressure levels, from 10 to 80 dB with 5-dB intervals. For each level, waveforms were amplified (gain 10,000), filtered (0.1–3 kHz), and averaged across 1,024 presentations. Threshold was determined with visual inspection of the waveforms. Amplitude and latencies of the ABR waveforms were analyzed using ABR Peak Analysis software.

Data analysis

Offline data analysis was performed using OriginPro 7.5 (Origin Laboratory). Liquid junction potentials (4 mV) were adjusted offline for all membrane potentials. Voltage-dependent steady-state I_h activation was analyzed by using the following Boltzmann equation:

$$G(V_m) = G_{\min} + \frac{G_{\max} - G_{\min}}{1 + e^{(V - V_{1/2})/s}}, \quad (1)$$

where G_{max} and G_{min} are the maximum and minimum conductance, $V_{1/2}$ is the voltage at half maximum activation and s is the slope factor.

I_h activation kinetics was examined by fitting the current evoked by a step to −144-mV potential with double exponential function:

$$I_h(t) = I_{ss} + I_f \exp(t/\tau_{fast}) + I_s \exp(t/\tau_{slow}), \quad (2)$$

where I_{ss} is the steady-state current at a given potential, I_s and I_f denote the amplitude of the slow and fast current components, and τ_{slow} and τ_{fast} are the corresponding time constants for I_h activation.

Statistical analysis was performed using OriginPro 7.5. All results were reported as means ± SD unless otherwise specified. Statistical analysis for I_h conductance (G_h), half-activation voltage ($V_{1/2}$), slope factor (s), and activation kinetics (τ_{fast}) were made using independent Student's *t* test. If comparison involved multiple genotypes, ANOVA was used followed by Dunnett's post-hoc test. 8-BrcAMP effect on I_h activation was analyzed using independent samples Student's *t* test. The effects of ZD7288, Ni_2Cl, and mibefradil on SGN firing properties were determined using paired Student's *t* test. Difference in means was considered significant if $P < 0.05$. Degree of scatter in spike time variation in response to small depolarizing current injection was quantified using confidence interval (CI) at 95%.

RESULTS

Spatiotemporal development of I_h in SGNs

To examine the contributions of HCN subunits to I_h in SGNs, we began with a qPCR analysis using primers that were selective for *Hcn1–4* and mRNA harvested from P3 WT SGN tissue. As shown in Fig. 1 A, the qPCR analysis indicated expression of *Hcn1*, *Hcn2*, and *Hcn4* in early postnatal SGNs. The total mRNA expression for *Hcn1*, *Hcn2*, and *Hcn4* per cochlea was 700,000:200,000:400,000, respectively, with little expression of *Hcn3*. When normalized to *Hcn3* mRNA copy number, the relative expression was as follows: *Hcn1-Hcn2-Hcn3-Hcn4* 21:6:1:12. Based on the expression ratio, it is evident that *Hcn1* was the most highly expressed in neonatal SGNs, followed by *Hcn4* and *Hcn2*. We speculate that the *Hcn3* expression in SGNs is minimal or nonexistent based on the low mRNA copy number; thus, its functional contributions in neonatal SGNs are likely to be negligible.

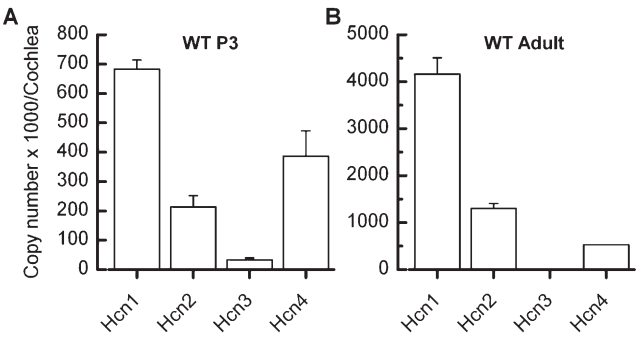

Figure 1. Expression of *Hcn* mRNA in mouse SGNs. (A and B) Expression of *Hcn1–4* in neonatal (A) and adult (B) WT mouse SGNs. qPCR was used to estimate the total mRNA copy number of *Hcn* genes present in both neonatal (P3) and adult stages (≥P40). Neonatal SGN samples were collected from a pool of 24 whole cochleas. Adult SGN samples were obtained from a pool of 16 whole cochleas. Each preparation was run in triplicate. Results are shown as mean total copies in thousands of *Hcn* mRNA transcripts per cochlea. Error bars represent SEM.

In adult SGNs our qPCR analysis of *Hcn* mRNA revealed expression of *Hcn1*, *Hcn2*, and *Hcn4* (Fig. 1 B). *Hcn1* was again the most highly expressed, with a significant increase in mRNA copy number relative to neonatal stages (Fig. 1, A and B). When normalized to *Hcn3*, the relative expression ratio was *Hcn1-Hcn2-Hcn3-Hcn4* 1,000:300:1:100. The data suggest that HCN1 is the principal subunit at both neonatal and adult stages.

To examine I_h in SGN cell bodies, we used the whole-cell, tight-seal technique in the voltage-clamp configuration to record from organotypic SGN explants acutely excised from neonatal mouse cochlea (P1–8). In response to 4-s hyperpolarizing voltage injections stepped from −74 to −144 mV in 10-mV increments from a holding potential of −84 mV, WT SGNs exhibited slowly activating inward currents. A representative family of current traces is shown in Fig. 2 A, in which the slowly activating inward current was detected at potentials negative to −84 mV and was fully activated at potentials negative to −124 mV. This current profile is characteristic of I_h in other neurons including SGNs (Chen, 1997; Mo and Davis, 1997; Yi et al., 2010) and was observed in every WT SGN we examined ($n = 143$).

To analyze the voltage dependence of I_h in WT SGNs, activation curves were generated by fitting a Boltzmann function (Eq. 1) to tail currents plotted as a function of step potential (Fig. 2 B). Tail currents were measured at the instant of a step to −84 mV, very close to potassium equilibrium potential (E_K). At −84 mV, contamination from potassium currents was minimal and other voltage-dependent currents were deactivated. WT SGNs ($n = 25$) had a mean maximum conductance (G_h) of 2.3 ± 0.8 nS and half-activation voltage ($V_{1/2}$) of −97.1 ± 4.1 mV (range: −91.2 to −106.0 mV) with a slope factor (s) of 5.9 ± 0.6 mV (range: 5.0–7.2 mV). These activation parameters were similar to those previously reported for I_h activation in SGNs of various species (Chen, 1997; Mo and Davis, 1997; Szabó et al., 2002; Yi et al., 2010).

WT SGNs showed a developmental increase in the amplitude of I_h during the first postnatal week (Fig. 2 D). We measured G_h between P1 and P8 and found a gradual increase as a function of age. This developmental increase in G_h in WT SGNs also reflected graded expression of I_h along the cochlear tonotopic axis (Fig. 2, C and D). Comparison of G_h from apical and basal cells within the same age groups (P1–4) revealed significantly larger G_h in basal than apical SGNs (Fig. 2 D). By the end of the first postnatal week, the tonotopic gradient had diminished.

I_h in neonatal SGNs is carried by HCN1, HCN2, and HCN4

To verify that the hyperpolarization-activated inward currents in WT SGN cell bodies were carried by HCN channels, we applied the HCN blocker ZD7288 during

voltage-clamp recordings and measured the change in I_h. We applied either 10 or 100 µM ZD7288 in the external bath and found that 10 µM blocked 47 ± 16% ($n = 4$) of the current at −124 mV, whereas 100 µM blocked 92 ± 4% ($n = 6$; Fig. 3). Complete I_h block was achieved 15 min after 100 µM ZD7288 treatment and the effect was irreversible. To confirm that the ZD7288 effect was selective for I_h, we subtracted a family of currents recorded in the presence of 100 µM ZD7288 (Fig. 3 B) from control currents (Fig. 3 A) recorded before application of the drug. The subtracted currents (Fig. 3 C) revealed that the ZD7288-sensitive currents were nearly identical in amplitude and activation kinetics to the control currents. Importantly, the subtracted currents did not include properties of any other current, suggesting that 100 µM ZD7288 is specific for I_h in SGNs. Although we have shown ZD7288 to be an I_h-specific antagonist (BoSmith et al., 1993; Harris and Constanti, 1995), it does not distinguish among the four HCN subunits. Thus, we wondered which HCN subunits contribute to the biophysical properties of I_h in WT SGNs. A previous study indicated localization of HCN1 and HCN4 subunits in rat SGN cell bodies at P9–10 (Yi et al., 2010); however, functional evidence implicating specific HCN subunits was not reported. Another study reported the presence of all four HCN subunits in adult guinea pig SGN cell bodies (Bakondi et al., 2009), raising the possibility that all four HCN subunits may be present in WT mouse SGNs.

To determine whether the *Hcn* mRNA expression patterns (Fig. 1) were translated into physiological expression of I_h, we recorded from SGNs excised from mice deficient in *Hcn1*, *Hcn2*, or both. Because our data and several in situ hybridization studies indicate very low expression levels of *Hcn3* mRNA (Ludwig et al., 1998; Moosmang et al., 1999), $Hcn3^{-/-}$ mice were not investigated. *Hcn4* is expressed in SGNs; however, $Hcn4^{-/-}$ mice are embryonic lethal (Stieber et al., 2003), and conditional $Hcn4^{-/-}$ mice are not available. Representative families of I_h recorded from SGNs of WT, $Hcn1^{-/-}$, $Hcn2^{-/-}$, and $Hcn1,2^{-/-}$ mice are shown in Fig. 4 A. Inward currents indicative of I_h were present in SGNs harvested from mice of all four genotypes. Current amplitudes and activation kinetics were noticeably diminished in $Hcn1^{-/-}$ SGNs relative to WT. $Hcn2^{-/-}$ SGNs showed reduced current amplitudes; however, their current activation kinetics was not significantly different from WT. In $Hcn1,2^{-/-}$ SGNs, in which both *Hcn1* and *Hcn2* were deficient, I_h was significantly reduced.

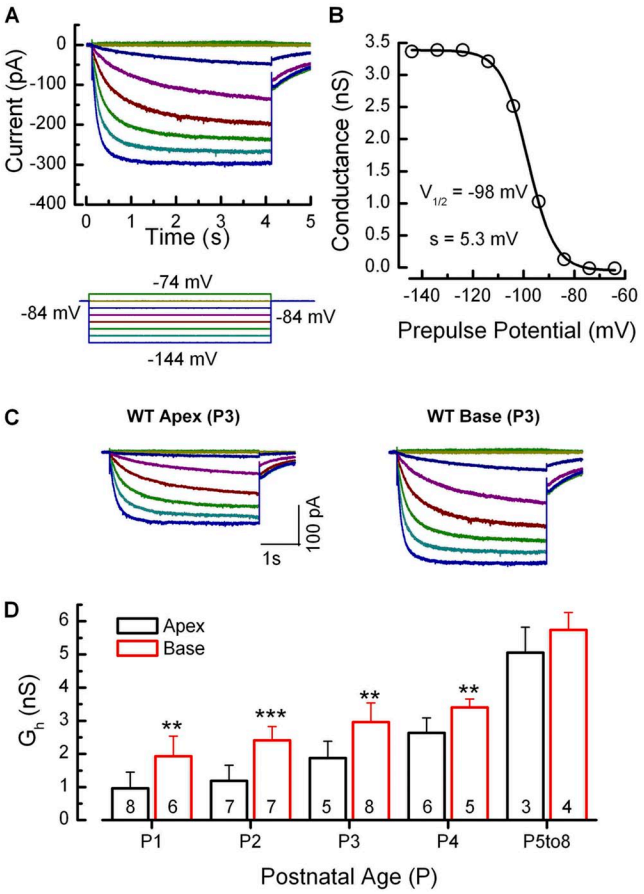

Figure 2. I_h in SGNs. (A) Representative current traces recorded from a WT SGN cell body (P3, base) in response to 4-s voltage steps from a holding potential of −84 mV to potentials between −144 and −74 mV in 10-mV increments. The bottom panel shows the voltage-clamp protocol. (B) A representative activation curve for G_h generated from the tail currents shown in A. Tail currents were divided by driving force (40 mV) and fitted with a Boltzmann function (black line; Eq. 1): $V_{1/2} = -98.3$ mV, s = 5.3 mV, and $G_h = 3.4$ nS. (C) Representative I_h traces of from apical and basal SGNs (P3) from the same cochlear explant. The scale bar applies to both current families. (D) Mean maximal conductance (G_h) plotted as a function of postnatal age and cochlear location (apex vs. base). Statistically significant differences (**, $P < 0.01$; ***, $P < 0.001$) indicated a tonotopic gradient (apex vs. base) during the first postnatal week. There was also a gradual, yet significant ($P < 0.001$), increase in G_h during the first postnatal week (mean of P0–4 relative to P5–8). Number of samples for each group is shown at the bottom. Error bars equal +1 SD.

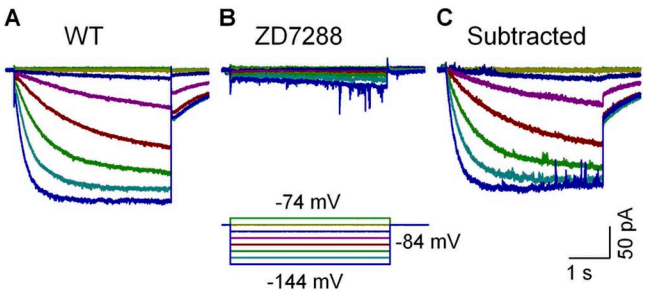

Figure 3. I_h in SGNs is carried by HCN channels. (A and B) Representative currents recorded from a WT, P2, basal SGN in response to hyperpolarizing voltage steps before (A) and after (B) 100 µM ZD7288 bath application. Voltage-clamp protocol is shown below. (C) Subtracted currents from datasets A and B show characteristics of I_h. The scale bar applies to all current families.

Representative activation curves are shown in Fig. 4 B. Relative to WT controls, the mean G_h was significantly ($P < 0.01$) reduced in both *Hcn1*$^{-/-}$ and *Hcn2*$^{-/-}$ SGNs, indicating expression of both HCN1 and HCN2 subunits contributes to I_h at early postnatal stages (Fig. 4 C). Reduction of G_h was most prominent in *Hcn1,2*$^{-/-}$ SGNs ($P < 0.001$). We suggest the larger reduction of G_h in *Hcn1,2*$^{-/-}$ SGNs is a consequence of simultaneous deletion of HCN1 and HCN2 subunits. The small residual I_h in *Hcn1,2*$^{-/-}$ was blocked by ZD7288, indicating the presence of other HCN subunits, most likely HCN4 (Fig. 4 A). In summary, the data suggest a prominent role for HCN1 with minor contributions from HCN2 and perhaps HCN4.

Analysis of G_h activation curves from *Hcn* mutant mice revealed additional evidence suggesting involvement of HCN1, HCN2, and HCN4 subunits in neonatal SGNs (Fig. 4, C–E). The mean voltage of half-activation was shifted in the negative direction in both *Hcn1*$^{-/-}$ and *Hcn1,2*$^{-/-}$ SGNs relative to WT ($P < 0.001$). *Hcn2*$^{-/-}$ SGNs also showed a slight but significant ($P < 0.05$) negative shift in $V_{1/2}$, raising the possibility that HCN2 makes a minor functional contribution in neonatal SGNs (Fig. 4 D). There were significant differences in the mean slope factors of *Hcn1*$^{-/-}$, *Hcn2*$^{-/-}$, and *Hcn1,2*$^{-/-}$ SGNs relative to WT, further supporting involvement of both HCN1 and HCN2 in neonatal SGNs (Fig. 4 E).

The kinetics of I_h activation was measured from double exponential fits to currents evoked by steps to −144 mV (Fig. 5 A). Fast time constants (τ_{fast}) were significantly ($P < 0.001$) slower in both *Hcn1*$^{-/-}$ (393 ± 123 ms; $n = 18$) and *Hcn1,2*$^{-/-}$ (522 ± 99 ms; $n = 8$) SGNs compared with WT (127 ± 47 ms; $n = 18$) and *Hcn2*$^{-/-}$ (134 ± 57 ms; $n = 19$) SGNs (Fig. 5 B). Similarly, slow time constants (τ_{slow}) were significantly ($P < 0.05$) slower in both *Hcn1*$^{-/-}$ (2,922 ± 2,168 ms; $n = 18$) and *Hcn1,2*$^{-/-}$ (2,993 ± 1,970 ms; $n = 8$) compared with WT (799 ± 901 ms; $n = 7$) and *Hcn2*$^{-/-}$ (951 ± 670 ms; $n = 19$).

In summary, the data from *Hcn*-deficient mice revealed I_h had significantly different biophysical properties in SGNs that lacked *Hcn1*. The differences included reduced current and conductance amplitudes, more negative $V_{1/2}$ values, and slower activation kinetics. These differences suggest that HCN1 subunits contribute to the

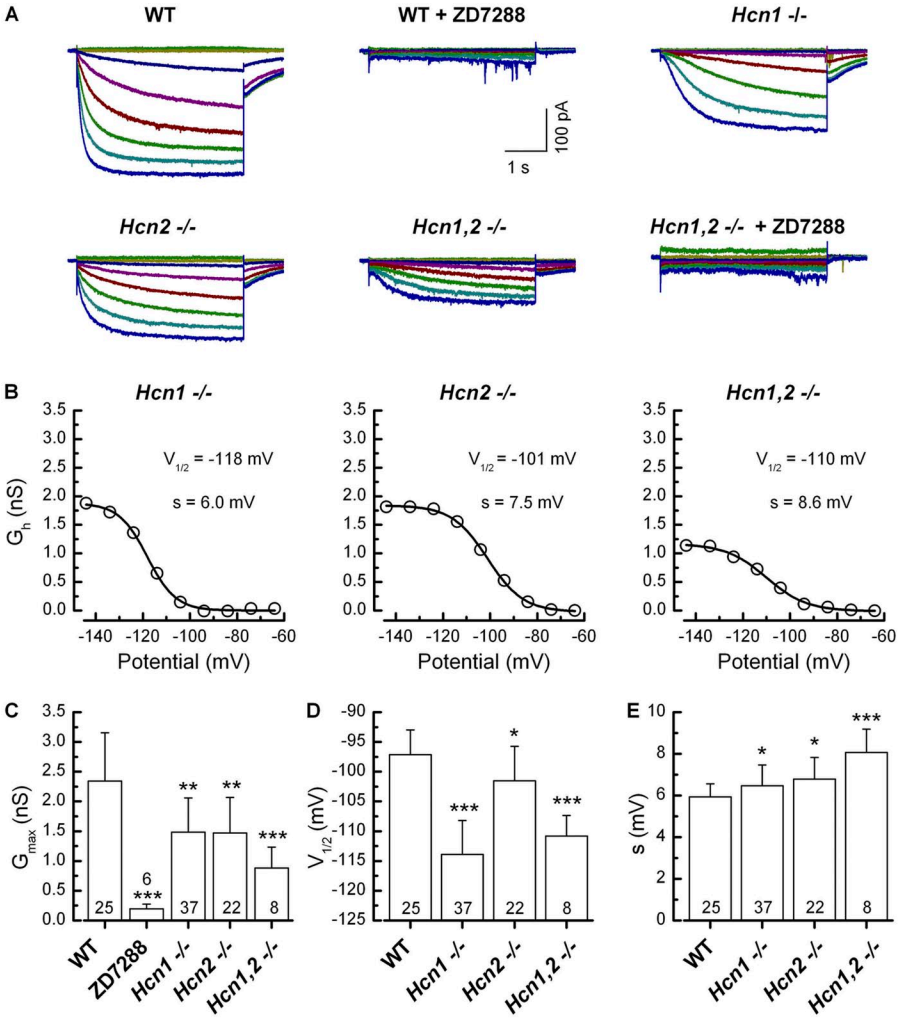

Figure 4. Biophysical characterization of I_h in neonatal (P1–4) WT and *Hcn*-deficient SGNs. (A) Family of representative I_h from WT, WT + 100 µM ZD7288, *Hcn1*$^{-/-}$, *Hcn2*$^{-/-}$, and *Hcn1,2*$^{-/-}$ SGNs as indicated. Currents were evoked using the same voltage-clamp protocol shown in Fig. 2. Residual currents in *Hcn1,2*$^{-/-}$ SGNs were blocked by 100 µM ZD7288. (B) Representative G_h activation curves for *Hcn1*$^{-/-}$, *Hcn2*$^{-/-}$, and *Hcn1,2*$^{-/-}$ SGNs fitted with Boltzmann equations. $V_{1/2}$ and s are indicated on the graphs. (C) Summary of mean maximal G_h. (D) Summary of mean half-activation voltage. (E) Mean slope factor. Number of samples and genotype are indicated below. Error bars equal +1 SD. *, $P < 0.05$; **, $P < 0.01$; ***, $P < 0.001$.

properties of I_h in SGNs. Interestingly, we found some differences in the properties of I_h in *Hcn2*$^{-/-}$ SGNs compared with WT, including reduction in G_h, a small negative shift in $V_{1/2}$, and a slight broadening of the activation curve, but no difference in kinetics, suggesting that the functional contributions of HCN2 to I_h in SGNs during early postnatal stages are minor relative to HCN1. Lastly, we suggest that small residual I_h in *Hcn1,2*$^{-/-}$ SGNs implies the presence of another HCN subunit. As *Hcn3* expression was shown to be minimal (Fig. 1 A), the small residual I_h is mostly likely caused by expression of *Hcn4*.

I_h is modulated by cAMP

HCN channel activity can be modulated by intracellular cyclic nucleotides (DiFrancesco, 1986; DiFrancesco and Tortora, 1991). Previous work in auditory brainstem neurons has shown that cAMP shifts I_h activation toward more depolarized potentials and speeds up activation kinetics (Banks et al., 1993; Yamada et al., 2005). To examine cAMP modulation of I_h in SGNs, we measured I_h activation after application of a membrane-permeable cAMP analogue, 8-Br-cAMP (200 µM), to the external bath (Fig. 6 A). In the presence of 8-Br-cAMP, the I_h activation range was shifted ($P < 0.001$) toward more depolarized potentials ($V_{1/2} = -88.5 \pm 0.6$ mV; $n = 4$) compared with control ($V_{1/2} = -95.3 \pm 0.3$ mV; $n = 4$; Fig. 6 B), with no increase in the maximal conductance. The 7-mV shift in $V_{1/2}$ in the presence of cAMP accounted for a 20% increase in I_h active at rest (approximately −80 mV). Similar results were found in rat SGN afferent dendrites, in which application of 200 µM 8-Br-cAMP resulted in a 12-mV positive shift in $V_{1/2}$ (Yi et al., 2010).

I_h in adult SGNs

We found a significant increase in the amplitude of I_h at adult stages, indicating developmental regulation (Fig. 7 A). Cultured WT SGNs ($n = 11$; apex, $n = 5$; base, $n = 6$) from adult mice P40 or older had a mean conductance of 13.4 ± 4.2 nS, which represented a sixfold increase in G_h compared with neonatal SGNs (P1–4, G_h = 2.3 ± 0.8 nS; $n = 25$). The tonotopic gradient in G_h expression during the first postnatal week (Fig. 2 D) was absent at adult stages (apex, 15.1 ± 5.8 nS; base, 12.0 ± 1.9 nS; P = 0.24), $V_{1/2}$ (apex, −94.9 ± 3.8 mV; base, −92.3 ± 6.3 mV; P = 0.44), and s (apex, 7.8 ± 1.8 mV; base, 7.8 ± 2.8 mV; P = 0.93).

Representative activation curves for adult WT and *Hcn*-deficient SGNs are shown in Fig. 7 B. Relative to adult WT SGNs, adult *Hcn1*$^{-/-}$ SGNs had significantly ($P < 0.001$) reduced mean G_h (Fig. 7 C), whereas *Hcn2*$^{-/-}$ SGNs had G_h values similar to WT. The $V_{1/2}$ values of adult *Hcn1*$^{-/-}$ were also significantly ($P < 0.001$) hyperpolarized compared with WT, whereas *Hcn2*$^{-/-}$ SGNs were not (Fig. 7, B and D). The slope factors were not significantly different between the three genotypes (not depicted). Activation kinetics of adult I_h was analyzed as described for neonatal I_h. Mean fast time constants (τ_{fast}) for WT, *Hcn1*$^{-/-}$, and *Hcn2*$^{-/-}$ SGNs are presented in Fig. 7 E. Interestingly, the activation kinetics (τ_{fast}) was significantly ($P < 0.01$) faster in adult WT neurons (57.3 ± 17.7 ms; $n = 11$) than in early postnatal neurons (127 ± 47 ms; $n = 18$). Yet, like the early postnatal cells, deletion of HCN1 subunits resulted in a significant slowing of I_h activation in adult SGNs (255.6 ± 67.3 ms; $n = 6$; $P < 0.01$),

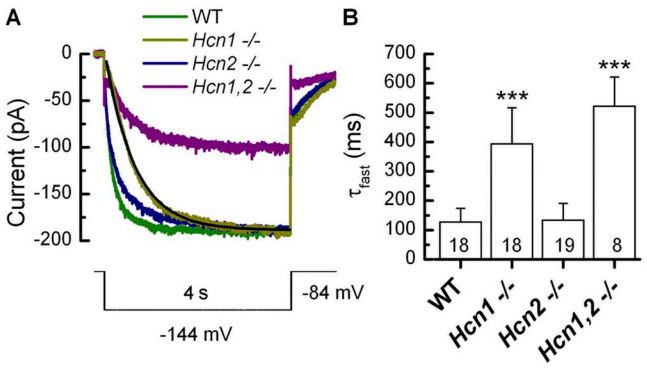

Figure 5. I_h activation kinetics (τ_{fast}) comparison in WT versus *Hcn*-deficient SGNs (P1–3). (A) Representative currents in WT, *Hcn1*$^{-/-}$, *Hcn2*$^{-/-}$, and *Hcn1,2*$^{-/-}$ in response to −144-mV voltage steps. I_h activation kinetics was measured by fitting a double exponential equation (black line; Eq. 2). (B) Summary of mean fast activation time constants. Number of samples and genotype are indicated below. Error bars equal +1 SD. ***, $P < 0.001$.

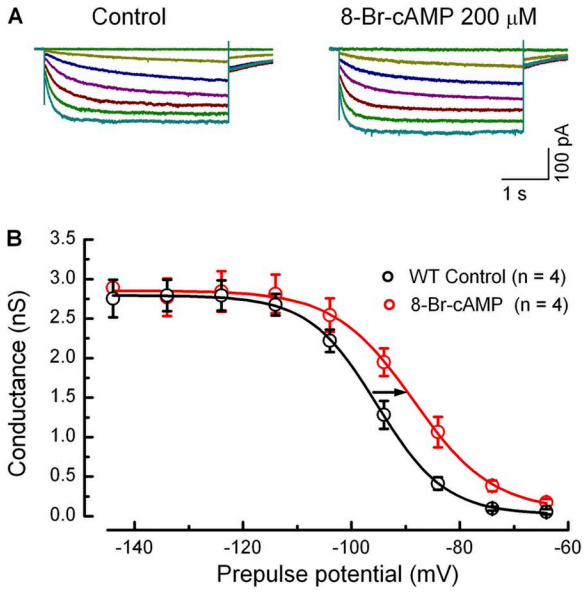

Figure 6. Modulation of I_h voltage dependence by cAMP. (A) Representative I_h traces from WT SGNs (P4, apex) in control (left) and after bath application of 200 µM 8-Br-cAMP (right). Recordings were made in two different cells from the same SGN explant tissue. Currents were evoked using the same voltage-clamp protocol shown in Fig. 2. (B) Mean voltage-dependent G_h activation curve from P3–4 SGNs. 200 µM 8-Br-cAMP was used. Data were fitted by a Boltzmann function. Note the shift in $V_{1/2}$ toward depolarized potentials with 8-Br-cAMP. Error bars equal ±1 SD.

whereas deletion of HCN2 subunits did not have a significant effect on fast activation kinetics (43.2 ± 16.4; $n = 11$) compared with WT. Likewise, mean slow activation time constants (τ_{slow}) were significantly ($P < 0.001$) prolonged in *Hcn1*$^{-/-}$ (2,209 ± 1,408 ms; $n = 6$) compared with WT (870 ± 699 ms; $n = 11$) and *Hcn2*$^{-/-}$ (611 ± 335 ms; $n = 11$). *Hcn1,2*$^{-/-}$ mice do not survive into adulthood and thus were not examined. The adult qPCR data (Fig. 1 B) are consistent with the voltage-clamp data (Fig. 7), which showed significant reduction (approximately sixfold) of G_h in *Hcn1*$^{-/-}$ SGNs, supporting the notion that HCN1 is the principal subunit contributing to I_h function in WT adult SGNs.

In summary, genetic deletion of *Hcn1* had qualitatively similar effects in neonatal and adult SGNs, indicating that HCN1 subunits are major components of I_h channels in both early postnatal and adult SGNs. Deletion of *Hcn2* was without significant effect at adult stages, raising the possibility that HCN2 contributions to SGN cell bodies may be transient. Doubly deficient *Hcn1,2*$^{-/-}$ mice did not live to adult stages, yet the similarity between residual I_h in neonatal *Hcn1,2*$^{-/-}$ SGNs and the small residual I_h in adult *Hcn1*$^{-/-}$ SGNs suggests the presence of additional HCN subunits, mostly likely HCN4 based on the qPCR analysis. The faster I_h activation kinetics at adult stages suggests that additional factors, perhaps intrinsic differences in endogenous cAMP levels, may also contribute to I_h function in adult SGNs.

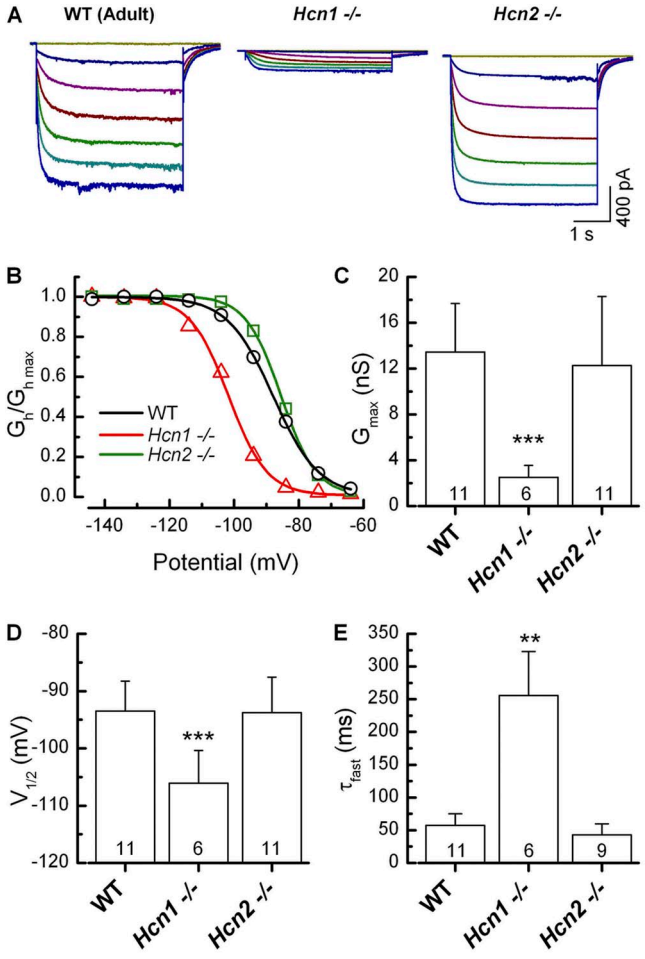

Figure 7. I_h expression in cultured adult SGNs. (A) Family of representative I_h traces from adult (≥P40, base) WT, *Hcn1*$^{-/-}$, and *Hcn2*$^{-/-}$ SGNs. (B) Normalized I_h activation curves generated by fitting a Boltzmann function to tail currents shown in A. Note the hyperpolarized half-activation voltage shift in *Hcn1*$^{-/-}$ SGNs compared with WT and *Hcn2*$^{-/-}$. (C and D) Summary of conductances (C) and half-activation voltages (D) for 11 WT, 6 *Hcn1*$^{-/-}$, and 11 *Hcn2*$^{-/-}$ SGNs. (E) Summary of I_h fast activation time constants. Error bars equal +1 SD. **, $P < 0.01$; ***, $P < 0.001$.

I_h contributes to resting potential

To examine the functional contributions of I_h to SGN membrane responses, we recorded from neonatal SGNs (P1–8) in current-clamp mode. Application of ZD7288 resulted in significant ($P < 0.05$) hyperpolarization of WT SGN resting membrane potentials (Fig. 8, A and B). The mean resting membrane potentials before and after bath application of 100 µM ZD7288 revealed a 6-mV hyperpolarization. The hyperpolarized resting membrane potential after ZD7288 treatment was similar to that of *Hcn1*$^{-/-}$ SGN resting membrane potentials (Fig. 8 A), whereas there was no significant difference in *Hcn2*$^{-/-}$ or *Hcn1,2*$^{-/-}$ SGNs. The data suggest that HCN1 subunits contribute depolarizing current that shifts the WT SGN resting membrane potential in the excitatory direction. The lack of resting potential effect in the *Hcn1,2*$^{-/-}$ SGNs was unexpected but may be a result of compensatory up-regulation of HCN4 subunits or some other depolarizing current as a consequence of genetic deletion of both *Hcn1* and *Hcn2*.

I_h contributes to sag and rebound potentials

To examine the contributions of I_h to membrane responses evoked by small input currents, we injected 5-pA hyperpolarizing currents for 2 s in WT SGNs. The membrane responded with a small fast hyperpolarization followed by a depolarizing "sag," which returned the membrane potential toward the resting level (Fig. 8 B). The 5-pA current injections were sufficient to produce prominent sag, while ensuring that the cell did not hyperpolarize negative to the physiological range, approximately −100 mV. The depolarization sag developed over ~150 ms, which reflected the slow activation kinetics (τ_{fast}) of WT I_h (Fig. 5). At the termination of the hyperpolarizing current step, a prominent rebound potential (10–15 mV; $n = 11$) was evident (Fig. 8 B, black trace).

To confirm whether these membrane responses were the result of I_h, we blocked I_h with bath application of 100 µM ZD7288 (Fig. 8 B). ZD7288 hyperpolarized the resting potential and abolished the depolarization sag (Fig. 8 B, red trace) with a difference of 11.6 ± 2.8 mV ($n = 10$) relative to control (Fig. 8 C). The sag was measured as the difference between the peak hyperpolarization and the steady-state potential near the end of the

current step (Fig. 8 B). The rebound potential was also abolished in the presence of ZD7288, indicating the contribution of I_h at the offset of the current step. (Fig. 8 B, red trace).

I_h contributes to SGN firing properties

The preceding data showed the involvement of I_h in shaping membrane responses to small current injections. Next, we investigated the functional contributions of I_h to AP firing in WT cells and in cells exposed to ZD7288. We used two different current-clamp conditions. In the first condition, APs were evoked from rest (I = 0) by injection of depolarizing currents in 2-pA increments. In the second condition, APs were evoked at the termination of 2-s membrane hyperpolarization to physiological levels (i.e., not exceeding −100 mV). In both conditions, AP threshold and latency were measured in the same cell before and after ZD7288 treatment. The current-clamp protocols were designed to allow systematic comparison of I_h contributions to SGN firing properties at rest, when HCN channels are partially active, and after hyperpolarization, when HCN channels are maximally activated within the physiological range.

As shown in Fig. 9 (A and B), an initial spike (at the onset of a depolarizing step) and a rebound spike (at the offset of a hyperpolarizing step) were evoked both before and after ZD7288 treatment. We found no significant difference in threshold for either the initial spike or the rebound spike, although the current required to evoke rebound spikes was less than that required for the initial spike (not depicted).

However, spike latency was significantly delayed for the rebound spike after treatment with ZD7288. Latency was measured as the time from the current step to the peak of first spike. There was a slight delay in the initial spike after ZD7288 exposure, but the latency difference after ZD7288 treatment (16.5 ± 7.7 ms; $n = 9$) was not statistically significant compared with control (15.2 ± 7.6 ms; $n = 9$; P = 0.08; Fig. 9, A [inset] and C). In contrast, there was a significant delay in the rebound spike in ZD7288-treated cells (P = 0.02) compared with control (Fig. 9, B [inset] and C). Blockage of I_h delayed the rebound spikes, on average, by 9.1 ± 9.6 ms.

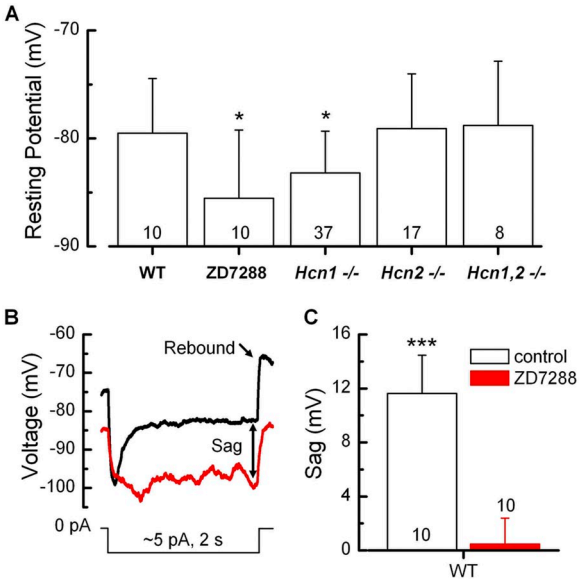

Figure 8. I_h contributes to neonatal (P1–8) SGN membrane responses. (A) Comparison of resting membrane potential (V_{rest}) before and after treatment with 100 µM ZD7288 in WT SGNs. Note that ZD7288 hyperpolarizes WT SGN V_{rest} to potentials comparable with that of *Hcn1*$^{-/-}$ SGNs. (B) Representative current-clamp recordings in WT SGNs (P3) in response to 2-s hyperpolarizing current (5 pA) injections. Note the depolarizing sag and rebound potential at the end of hyperpolarizing current step in the control condition (black trace). In the presence of 100 µM ZD7288, the depolarization sag and rebound potential are abolished (red trace). (C) Quantification of sag amplitude before and after treatment with 100 µM ZD7288 from the same cells. Sag amplitude was measured as the difference between the peak hyperpolarization and the steady-state potential near the end of the current step. Error bars equal +1 SD. *, P < 0.05; ***, P < 0.001.

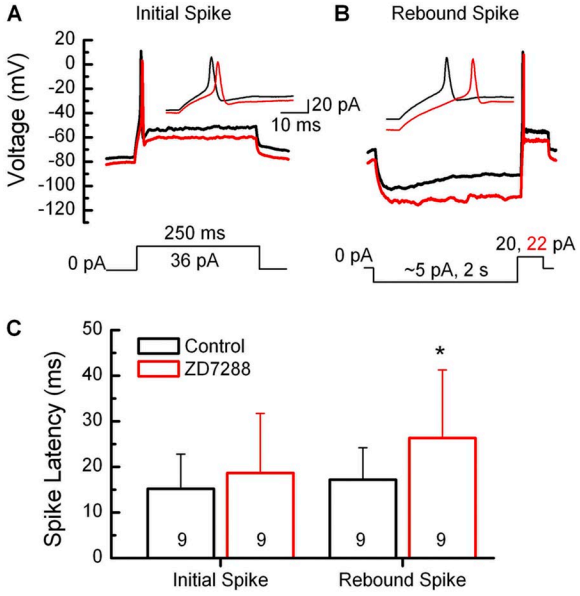

Figure 9. I_h modulates firing properties in SGNs. (A) Representative traces (P1, apex) showing AP firing in WT SGNs in two different conditions. An initial spike was evoked from resting membrane potential (I = 0) by injecting depolarizing currents in 2-pA increments until threshold was reached (current-clamp protocol below). (B) Representative rebound spikes (P1, apex) were evoked after hyperpolarization of the membrane to potentials within the physiological range (at least −100 mV). Both initial spikes and rebound spikes were examined in the same cell. For each condition, representative recordings obtained in control (black traces) and in the presence of 100 µM ZD7288 (red traces) were superimposed for comparison. The insets show the same spike pairs on an expanded time scale. (C) Comparison of spike latency for initial spikes and rebound spikes (P1–3) before (black) and after 100 µM ZD7288 application (red). Error bars equal +1 SD. *, P < 0.05.

To investigate the possibility that the delay in the rebound spike may have been affected by activation of low-voltage–activated calcium channels, we used bath application of the calcium channel blockers, nickel (100 µM) or mibefradil (2 µM), either alone or together with 100 µM ZD7288. Neither nickel nor mibefradil alone affected rebound spike latency, as no difference was found before (control) and after treatment (Fig. 10, A–C). However, when ZD7288 was added subsequently, there was a significant ($P < 0.01$) delay in the rebound spike, again indicating that I_h and not low-voltage–activated calcium channels is a significant contributor for rebound spike timing in SGNs (Fig. 10, A–C).

To investigate whether the I_h effects on resting potential, sag potential, and spike latency were caused by HCN1 or HCN2, we examined adult SGNs of WT, *Hcn1*$^{-/-}$, and *Hcn2*$^{-/-}$ mice. SGNs from adult *Hcn1*$^{-/-}$ mice had resting potentials that were significantly more hyperpolarized than both WT and *Hcn2*$^{-/-}$ SGNs (Fig. 11 A). Hyperpolarizing current steps evoked a prominent sag (Fig. 11 B) that decayed more quickly than the sag recorded from neonatal SGNs (Fig. 8 B), consistent with the faster I_h activation kinetics in adult SGNs (Fig. 7 E). The amplitude of the sag potential was also significantly reduced in adult *Hcn1*$^{-/-}$ SGNs relative to WT and *Hcn2*$^{-/-}$ SGNs (Fig. 11 C). Lastly, we noted a delay in rebound spike latency in adult *Hcn1*$^{-/-}$ SGNs (Fig. 11, B and D), which confirms a prominent role for HCN1 in spike timing in adult SGNs.

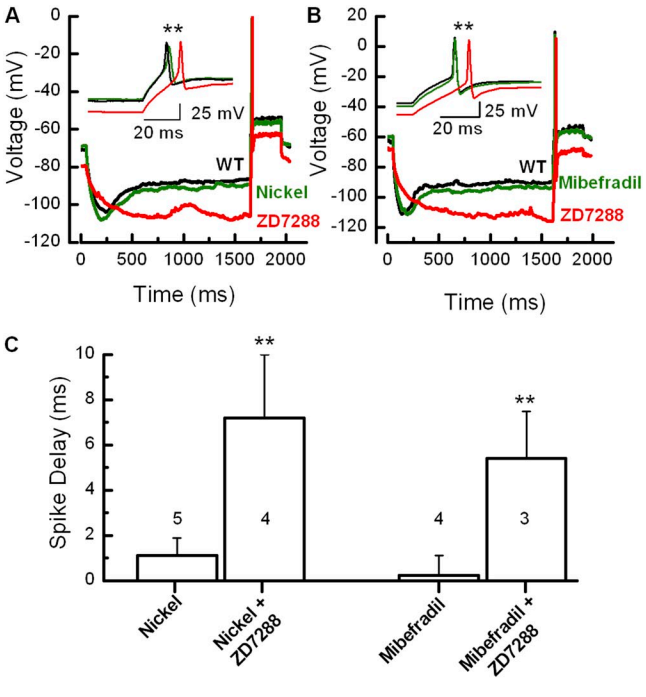

Figure 10. I_h regulates rebound spike latency. (A) Representative traces of rebound spikes recorded from a WT SGN (P3, base) in three different conditions, control, 100 µM nickel, and both nickel and 100 µM ZD7288. Note that calcium channel blocker, nickel, had little effect on resting membrane potential, sag potential, and rebound spike latency (inset). However, subsequent block of I_h by ZD7288 abolished the depolarizing sag and delayed the rebound spike (inset). (B) Representative traces of rebound spikes recorded in WT control conditions, with 2 µM mibefradil, and with mibefradil and 100 µM ZD7288. Here again, the T-type calcium channel blocker had little effect on resting membrane potential, sag potential, and rebound spike latency (inset), whereas ZD7288 hyperpolarized the cell, blocked the sag potential, and delayed the rebound spike. (C) Spike delay was measured as the difference between spike peaks in WT control conditions and after application of the drugs indicated below. Number of cells is indicated on the bar graph. Error bars equal +1 SD. **, $P < 0.01$.

I_h contributes to synchronized firing

To address the extent to which tonically active I_h contributes to AP firing, we delivered a series of 20 AP threshold current steps in WT SGN cell bodies before and after bath application of 100 µM ZD7288. Before ZD7288 treatment, SGNs exhibited little variation in spike latency for a threshold stimulus (Fig. 12 A, black traces). After application of ZD7288, we found both an AP delay and a larger distribution in spike latency (Fig. 12 A, red traces), suggesting that I_h active at rest contributes to the regularity of spike timing. To examine the contributions of I_h to the AP wave form, the spikes shown in Fig. 12 A were aligned with their peaks at time 0 and averaged. The averaged spikes before and after application of ZD7288 (Fig. 12 B) revealed that I_h functions to speed the depolarization to threshold and depolarize the membrane during the after hyperpolarization but does not affect the peak or rising/falling phases of the AP. Spike latency was also delayed and with greater distribution for small super-threshold stimuli of 30–40 pA (Fig. 12 C), but the effect was absent for larger stimuli (≥50 pA). The data support the notion that I_h helps shape the membrane response to small current steps, has significant impact on AP latency, and functions to enhance synchronized firing in response to small depolarizing stimuli.

I_h contributes ABR latency

Given that the results presented in the previous sections show HCN1 subunits carry a significant fraction of I_h in both neonatal and adult SGNs and that I_h contributes to resting membrane potential, spike latency, and synchrony, we wondered whether I_h may contribute to auditory processing. Behavioral deficits in auditory function have not been reported in previous studies of *Hcn*-deficient mice (Ludwig et al., 2003; Nolan et al., 2003, 2004; Herrmann et al., 2007). As none of these prior studies focused on auditory function, we decided to measure ABRs to sound stimuli in adult *Hcn1*$^{-/-}$ mice and their WT littermate controls. We restricted our analysis to the first peak of the ABR waveform, which represents the summed activity of the eighth cranial nerve. Relative to WT littermate controls, *Hcn1*$^{-/-}$ mice showed no difference in threshold (Fig. 13 A) or amplitude (Fig. 13 B), indicating that

auditory sensitivity and the number of responsive SGNs was unaffected. However, we did notice that *Hcn1*$^{-/-}$ mice showed longer compound AP latencies at several stimulus intensities (Fig. 13 C). As temporal fidelity is a critical parameter for auditory processing, we suggest that differences in latency at the level of the single SGN AP and in the ABR waveform may have significant consequences for normal sound processing.

DISCUSSION

We characterized I_h in SGN cell bodies harvested from neonatal (P1–8) and adult (≥P40) mice using the whole-cell, tight-seal technique. Biophysical analysis of I_h in WT and *Hcn*-deficient mice indicated a prominent role for HCN1 subunits as major carriers of I_h in SGNs. *Hcn1*$^{-/-}$ SGNs exhibited significantly reduced conductances (G_h), hyperpolarized half-activation voltages ($V_{1/2}$), and slow activation kinetics (τ_{fast}). qPCR analysis of *Hcn* mRNA revealed strong expression of *Hcn1* in both neonatal and adult SGNs, strengthening the notion that HCN1 is a major functional subunit underlying I_h in SGNs. I_h in SGNs is partially active at the cell's resting membrane potential and its activation increases with hyperpolarization. Here we present evidence that I_h contributes to SGN resting membrane potentials and firing properties, as blockage of I_h hyperpolarized the resting potential, abolished depolarization sag potentials, delayed rebound spikes, and increased variance in spike latencies. Furthermore, *Hcn1*$^{-/-}$ mice showed longer ABR latencies, further supporting the view that HCN1 subunits contribute to AP firing patterns and high-fidelity auditory information transfer between the periphery and the brain.

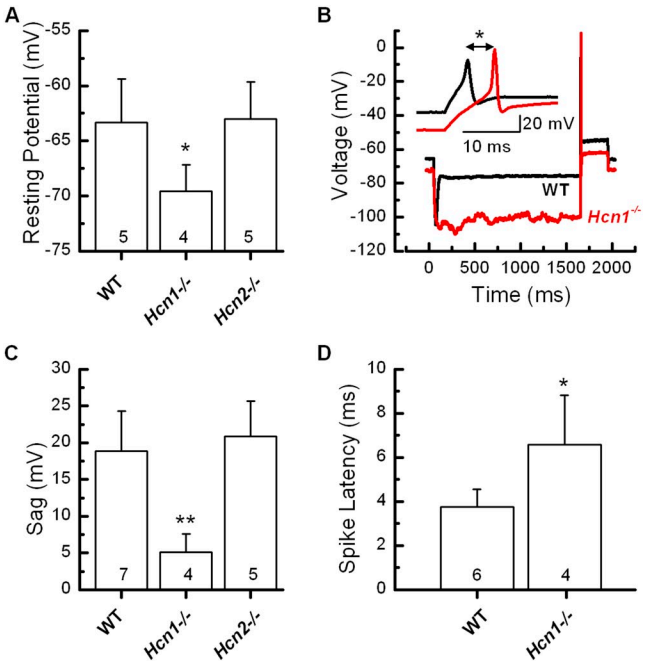

Figure 11. HCN1 contributes to membrane properties in adult SGNs. (A) Mean resting potentials recorded from 14 adult SGNs of the indicated genotypes. Number of cells for each genotype is indicated below. *, $P < 0.05$. (B) Representative membrane responses to hyperpolarizing currents steps recorded from adult WT and *Hcn1*$^{-/-}$ SGNs. The inset shows the rebound spike on an expanded time scale. (C) Sag potential was significantly (**, $P < 0.01$) diminished in adult *Hcn1*$^{-/-}$ SGNs. (D) Mean rebound spike latency for adult *Hcn1*$^{-/-}$ SGNs showed a significant delay relative to WT SGNs (*, $P < 0.05$). Error bars equal +1 SD.

SGN I_h is developmentally regulated

SGNs express various voltage-dependent currents (Adamson et al., 2002; Chen et al., 2011) in a manner that may serve to enhance developmental mechanisms throughout the first postnatal week until the onset of hearing, P10–12 (Romand, 1983). Consistent with this notion, we found that I_h in SGNs is developmentally

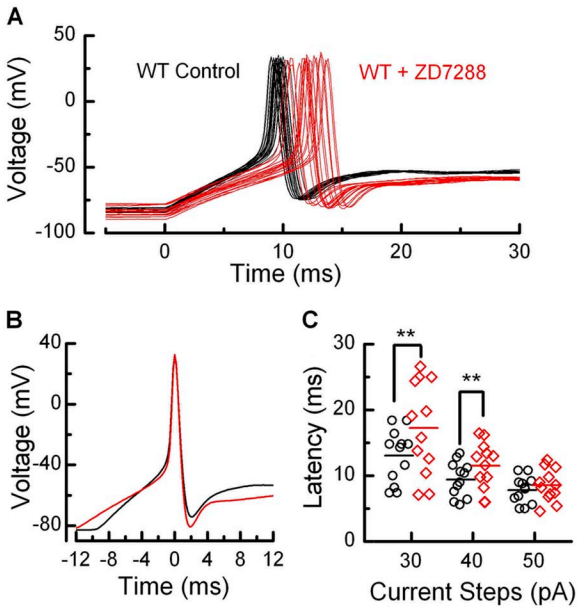

Figure 12. I_h contributes to synchronized AP firing in response to small depolarizing currents. (A) Representative APs measured from the same WT SGN (P4, apex) before (black traces) and after treatment with 100 µM ZD7288 (red traces). For each condition, a series of 20 APs were evoked using threshold current steps. Note the delay and larger distribution in spike latency after application of ZD7288. (B) Representative averaged (P4, apex) spike waveforms before (black trace) and after ZD7288 (red trace). Spikes were aligned with their peaks at time 0 and averaged. (C) Scatter plot showing spike latency for three different current injections from the same 12 cells (P1–4) before (black symbols) and after treatment with 100 µM ZD7288 (red symbols). The mean latency is indicated by horizontal lines (**, $P < 0.01$). Note the variation in spike latency is significantly increased for small depolarizing current steps (30 and 40 pA) in the presence of 100 µM ZD7288 but is minimal for larger steps (≥50 pA). CI (95%) of mean difference was used to quantify the degree of variation in spike latency before and after treatment with ZD7288. 30 pA: 1.55 < CI 95% < 6.83 ms; 40 pA: 0.93 < CI 95% < 3.18 ms; 50 pA: 0.28 < CI 95% < 1.70 ms.

regulated. Whole-cell voltage-clamp recordings from WT SGN cell bodies revealed a gradual increase in G_h over the first postnatal week. Because of myelination of SGN cell bodies (Romand and Romand, 1987; Echteler, 1992), which presents a technical limitation for whole-cell electrophysiological recordings, we did not attempt to record from SGNs beyond P8, a time point after which myelination becomes prohibitively thick and the bony labyrinth encapsulating SGNs becomes fully calcified. Although our recording time frame (P1–8) does not provide the full view of SGN I_h development, it did reveal a clear pattern leading up to the onset of hearing. Because synaptogenesis and mature innervation patterns between IHCs and SGNs are nearly complete by the end of the first postnatal week (Simmons et al., 1991; Pujol et al., 1998), it is likely that early postnatal development of I_h in SGNs impacts maturation of the auditory system before the onset of hearing.

The lack of I_h data around the onset of hearing raises the possibility that the developmental trend we noted is a transient phenomenon. However, our data from cultured adult SGNs indicate that I_h expression is sustained into adulthood. Previous studies that showed the presence of I_h in dissociated adult guinea pig SGN culture (Chen, 1997; Szabó et al., 2002) support this view.

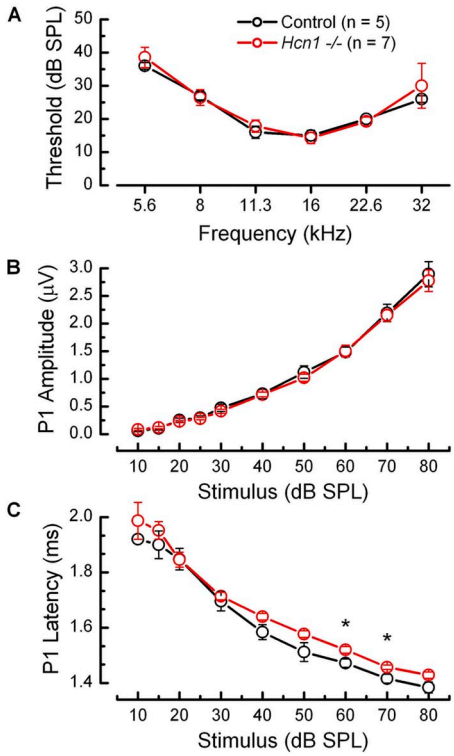

Figure 13. *Hcn1*$^{-/-}$ animals have delayed ABR latency. (A) Mean ABR thresholds for control and *Hcn1*$^{-/-}$ animals at 6–7 wk of age. (B and C) Mean wave 1 (P1) amplitude (B) and mean wave 1 (P1) latency responses (C) evoked by 16-kHz tone pips delivered across increasing sound stimulus intensity. Note that *Hcn1*$^{-/-}$ mice show delayed P1 latency relative to controls, whereas no significant difference was found in threshold (A) or amplitude (B). Error bars equal ±1 SEM. *, $P < 0.05$.

Tonotopic expression of I_h in SGNs

An important task of the auditory system is decomposing complex sound into constituent frequencies along the tonotopic axis of the organ of Corti. IHCs located in the basal part of the cochlea encode high-frequency sound, whereas those located in the apical region encode low-frequency sound. The tonotopic specialization is retained at each level along the ascending auditory pathway, including SGNs which are organized to reflect the tonotopic arrangement of IHCs (Rubel and Fritzsch, 2002). To enable this tonotopic arrangement, SGNs are equipped with morphological and electrophysiological specializations, including graded expression of voltage-gated channels (Adamson et al., 2002; Lv et al., 2010, 2012; Chen et al., 2011).

In the present study, we found that I_h in neonatal WT SGNs is also graded along the cochlear tonotopic axis, with greater I_h amplitudes in neurons from the basal end of the cochlea. Considering the graded expression of other voltage-gated channels in neonatal SGNs (Adamson et al., 2002; Chen et al., 2011), it seems I_h follows this trend. However, because the cochlea develops from base to apex, we cannot exclude the possibility that the graded I_h expression we report here for neonatal SGNs might be a transient phenomenon reflecting the developmental lag between the cochlear base and apex. Indeed, at adult stages, we noted little difference between I_h of basal and apical SGNs. Nonetheless, if larger I_h in SGNs from the basal, high-frequency end persists in the interval between P8 and more mature stages, we predict it will contribute to enhanced spike timing. Similar trends have been shown in neurons of the medial nucleus of trapezoid body, higher-order auditory neurons in the brainstem, in which graded I_h expression with high to low expression along the mediolateral (high to low frequency) axis results in a gradient of time delays in neuronal firing (Leao et al., 2006).

Characterization of I_h in mouse SGNs

The biophysical properties of I_h in WT SGNs in the present study are consistent with those previously reported for I_h in the auditory system, including SGNs (Chen, 1997; Mo and Davis, 1997; Szabó et al., 2002; Yi et al., 2010) and auditory brainstem neurons (Banks et al., 1993; Bal and Oertel, 2000). WT SGN I_h was a ZD7288-sensitive, slowly activating, noninactivating inward current evoked by hyperpolarizing voltage steps. SGN I_h was active at the cell's resting potential, and its activation range was well fit by Boltzmann functions with parameters ($V_{1/2}$ = −97 mV and s = 6 mV) similar those reported for SGN I_h in previous studies of various rodent species (guinea pig: $V_{1/2}$ = −101 mV and s = 9 mV [Chen, 1997]; and $V_{1/2}$ = −104 mV and s = 6 mV [Szabó

et al., 2002]; mice: $V_{1/2}$ range = −83 to −109 mV and s range = 7.6–13.1 mV [Mo and Davis, 1997]; and rat: $V_{1/2}$ = −104 mV and s = 11 mV [Yi et al., 2010]). These biophysical and pharmacology properties are consistent with the notion that I_h in SGNs is carried by HCN subunits. Although one prior study presented immunolocalization data suggesting the presence of HCN1, HCN2, and HCN4 subunits in rat SGNs (Yi et al., 2010), none presented definitive physiological evidence identifying the precise HCN subunits involved.

Expression of HCN1, HCN2, and HCN4 in neonatal SGNs

Given their complex heterogeneous biophysical properties, identification of HCN subunits mediating SGN I_h is challenging, yet critical for a comprehensive understanding of their functional relevance. Through qPCR analysis and examination of biophysical properties of I_h in *Hcn*-deficient animals, we demonstrated that I_h in neonatal SGNs is carried by HCN1, HCN2, and HCN4 subunits, with HCN1 being the most prominent subunit. Deletion of *Hcn1* resulted in significant reduction in I_h, hyperpolarized half-activation voltage, and slower activation kinetics. The biophysical differences we noted in neonatal *Hcn1*-deficient SGNs are consistent with those of HCNs expressed in various heterologous systems. Homomeric HCN1 channels have the fastest activation kinetics and most depolarized half-activation range (Santoro et al., 2000; Ishii et al., 2001; Altomare et al., 2003), whereas homomeric HCN4 channels show the slowest activation kinetics (Ludwig et al., 1999; Ishii et al., 2001). Homomeric HCN2 channels exhibit activation kinetics intermediate to HCN1 and HCN4 (Ludwig et al., 1999). In our study, I_h in *Hcn2*$^{-/-}$ SGNs had reduced amplitudes and a negative shift in the half-activation voltage; however, the differences were not as striking as those between *Hcn1*$^{-/-}$ and WT SGNs, suggesting that the functional contributions of HCN2 subunits are minor. The low expression levels of *Hcn2* mRNA in neonatal SGNs also suggested a small contribution from *Hcn2*. Previous immunolocalization work (Yi et al., 2010) demonstrated HCN2 immunoreactivity in P20 rat SGNs, but earlier time points were not examined. Thus, it is unclear whether there are actual differences in the temporal expression pattern of HCN2 or differences between rodent species. Yi et al. (2010) also reported robust expression of HCN1 and HCN4 in rat SGN cell bodies at P9–10. Their HCN1 and HCN4 localization data are consistent with our qPCR and electrophysiological data, and both studies suggest contributions from HCN1 and HCN4 before the onset of hearing at P10–12.

HCN1 contributes to I_h in adult SGNs

Analysis of mRNA expression in neonatal SGNs indicated that *Hcn1* is the most abundantly expressed subunit, followed by *Hcn4* and *Hcn2*. Strong *Hcn1* expression persisted into adult stages, suggesting HCN1 as the major subunit in adult SGNs. Our qPCR data are in agreement with *Hcn1* gene expression results from the SHIELD database (Shared Harvard Inner-Ear Laboratory Database; Lu et al., 2011). This database incorporates RNA gene chip sequencing information from SGNs harvested from mice expressing GFP under an SGN-specific MafB promoter at several developmental time points (embryonic day 16, P0, P4, P7, and P16). Among the three *Hcn* genes (*Hcn1*, *Hcn2*, and *Hcn3*) examined, *Hcn1* showed the strongest signal with a gradual developmental increase, consistent with our findings.

The strongest evidence supporting a prominent role for HCN1 in adult SGNs is derived from our voltage-clamp data, which showed an ∼80% reduction in G_h in SGNs from adult *Hcn1*$^{-/-}$ mice relative to WT. There was also significant difference in half-activation voltage and activation kinetics (τ_{fast}) relative to WT, strengthening the notion that HCN1 is indeed a major subunit contributing to I_h function in adult SGNs. There was no difference in I_h of adult SGNs from *Hcn2*$^{-/-}$ mice relative to WT, suggesting HCN2 does not contribute at adult stages. The qPCR data suggested expression of *Hcn4* at adult stages; however, in the absence of electrophysiological data supporting this result, we are reluctant to draw conclusions about functional contributions of *Hcn4* in adult SGNs.

I_h contributes to SGN membrane potential

I_h has been shown to contribute to resting membrane potentials by providing inward current at rest. We demonstrated I_h has a similar role in resting membrane potentials in SGN cell bodies, as acute block of I_h with ZD7288 resulted in significant resting potential hyperpolarization (−6 mV) in WT SGNs. Similar results were reported for postnatal rat SGN dendrites, which had a −4-mV hyperpolarization after ZD7288 treatment (Yi et al., 2010). I_h contribution to resting potential has also been observed in higher-order auditory neurons, such as cochlear nucleus and inferior colliculus, where inhibition of I_h resulted in similar resting membrane potential hyperpolarization (Bal and Oertel, 2000; Koch and Grothe, 2003; Nagtegaal and Borst, 2010).

In WT neurons, depolarization of the resting membrane potential is caused by tonic activation of I_h at rest. Based on the SGN I_h activation curve, we estimate that ∼5% of I_h is active at rest at neonatal stages and ∼20% at adult stages, suggesting an I_h contribution may be greater at adult stages. Because the reversal potential of I_h in SGNs is more positive than the cell's resting membrane potential (Chen [1997]: −36 mV; Mo and Davis [1997]: −41 mV; and Yi et al. [2010]: −45 mV), the resulting inward current drives the membrane toward more depolarized voltages. The tonic inward current produced by I_h in SGNs is most likely mediated through HCN1 subunits, as *Hcn1*$^{-/-}$ SGNs exhibited hyperpolarized resting membrane potential similar to WT cells treated with ZD7288.

Given that SGNs are critical for high-fidelity information transfer between IHC and central neurons in the auditory pathway, the functional significance of I_h in SGNs is clear. Because APs are generated at the spike initiation zone close to the IHC-SGN afferent synapse, it could be argued that the role of the cell body may be minor for auditory signal propagation. Recently, Yi et al. (2010) showed the presence of I_h in SGN afferent dendrites and its contribution to shortening the EPSP (excitatory postsynaptic potential) waveform at the IHC-SGN synapse. We suggest I_h in SGN cell bodies may also contribute to signal propagation from afferent terminals to central axons. SGNs are bipolar with large cell bodies positioned between dendrites and axons, which may present a problem for signal propagation (Hossain et al., 2005). The large SGN cell body may behave as an electrical sink, where the electric load may cause impedance mismatch, which in turn could interfere with rapid and efficient signal propagation from dendrite to axon. One mechanism for overcoming this electrical challenge in SGNs is expression of ion channels at peripheral and central initial segments flanking SGN cell bodies (Hossain et al., 2005). Indeed, SGNs express several varieties of voltage-gated channels (Santos-Sacchi, 1993; Szabó et al., 2002) that may help enhance current density in the cell bodies. Given that HCN channels are also expressed in SGN cell bodies, it is plausible that the tonic activation of I_h at rest may provide an extra "boost" by depolarizing the resting membrane potential and thereby enhancing auditory signal transmission.

I_h contributes to spike timing

We found that I_h activation modulates SGN firing properties. Here we show that activation of I_h by physiologically relevant hyperpolarizing currents induced depolarizing sag potentials and enhanced rebound potentials in SGNs. The depolarization sag, with a time course that reflects I_h activation kinetics, slowly restored membrane potentials toward the resting potential. The rebound potentials at the end of hyperpolarizing steps enhanced membrane depolarization, bringing the cell closer to threshold for AP generation. During ZD7288 inhibition of I_h, the depolarizing sag and rebound potentials were completely abolished, suggesting that activation of I_h provides subthreshold inward currents that enhance SGN excitability. We have extended this observation in adult SGNs to show that HCN1, in particular, contributes to depolarizing sag potentials, enhanced rebound potentials, and shorter rebound spike latencies.

Previous studies indicated that additional factors may contribute to rebound spikes such as low-voltage–activated T-type calcium channels (Aizenman and Linden, 1999, Lüthi and McCormick, 1998). Upon hyperpolarization, T-type calcium channels can recover from inactivation, making them available to open and enhance rebound potentials. Recent studies demonstrated that I_h and low-voltage–activated T-type calcium channels act in concert to enhance rebound spike timing in auditory brainstem neurons (Felix II et al., 2011; Kopp-Scheinpflug et al., 2011). As T-type calcium channels have been identified in murine SGNs (Chen et al., 2011; Lv et al., 2012), we wondered whether rebound spike timing in SGNs is caused by I_h alone or functions in concert with T-type calcium channels. We found that neither nickel, a broad spectrum calcium channel inhibitor, nor mibefradil, a T-type channel blocker, affected the depolarization sag or rebound spike timing. Thus, we conclude that I_h is a prominent contributor to rebound spike timing in SGNs with little contribution from calcium channels.

I_h also contributes to synchronized AP firing in response to small depolarizing stimuli. In the presence of ZD7288, the scatter in AP spike timing increased significantly for small depolarizing stimuli. The effect became less pronounced for larger depolarizing stimuli. We reason that synchronous firing in response to small depolarization is a direct consequence of tonic I_h activation at rest, which provides additional inward current, thereby driving membrane potentials toward the AP threshold more quickly. For larger depolarizing stimuli, I_h is reduced as membrane potential is driven closer to the I_h reversal potential and the relative contribution of I_h is diminished as a result of enhanced activation of voltage-gated sodium channels. Thus, I_h is most influential for small membrane potential deviations around the SGN resting potential.

Given the slow activation kinetics, it is unlikely that I_h can follow rapid membrane potential changes at auditory frequencies. Rather than following hair cell receptor potentials on a cycle by cycle basis, it is more likely that the tonic activation of I_h helps shape the direct current component of auditory signal processing by depolarizing the resting SGN membrane potential, leading to synchronized AP firing.

During development, however, the slow activation kinetics of I_h may suit the system. Before the onset of hearing (P12), IHCs fire recurrent Ca^{2+} APs at a very low discharge rates (2–4 HZ; Kros et al., 1998), which are hypothesized to drive spontaneous activity in SGNs during development (Tritsch et al., 2007; Tritsch and Bergles, 2010). Considering the tonotopic and developmental regulation of I_h in SGNs as shown in the present study, it is possible that I_h primes SGNs to faithfully follow the recurrent Ca^{2+} spikes from IHCs during development (Tritsch et al., 2007; Tritsch and Bergles, 2010; Johnson et al., 2011).

Contributions of SGN I_h to auditory function

Our results indicate that I_h contributes to SGN firing properties by regulating rebound spike timing and enhancing synchronized AP firing in response to small

depolarizing stimuli. If so, what is the functional significance of I_h for auditory processing? Because SGNs relay auditory information from the IHCs to higher-order auditory neurons via the eighth cranial nerve, our ABR data from *Hcn1*$^{-/-}$ mice, which indicate measureable delays in the latency of auditory signals, suggest that HCN1 helps preserve temporal fidelity in the eighth cranial nerve.

Accurate and precise transmission of IHC signals with high temporal fidelity is critical for normal auditory information processing. Thus, we propose I_h has a role in ensuring temporal precision, particularly for faint auditory signals. Although we did not detect differences in ABR threshold in *Hcn1*$^{-/-}$ mice, I_h may serve to boost sensitivity to faint auditory stimuli. In the mature auditory system, SGNs innervate IHCs in a 1:1 ratio (i.e., each SGN contacts only one IHC), whereas each IHC is innervated by groups of 20–30 SGNs (Liberman, 1982). This IHC-SGN innervation pattern ensures the activity of each SGN is strictly dependent on the activity of just one presynaptic hair cell and that each hair cell can drive the activity of multiple SGNs. Our findings suggest that I_h enhances synchronized AP firing to small depolarizing stimuli both within a single neuron and across a population of neurons. Thus, in response to slight changes in the membrane potential of a single IHC, SGN I_h enhances the likelihood of triggering synchronous APs in populations of SGNs. Synchronous firing, with reduced temporal jitter, across a population of neurons can help preserve temporal fidelity and enhance signal to noise ratios, particularly for small stimuli. Preservation of these signals may allow higher-order auditory centers to extract relevant faint signals from a noisy background. Thus, I_h in SGNs may serve to enhance temporal fidelity and boost sensitivity to soft sounds.

Yi et al. (2010) showed that I_h in the postsynaptic SGN dendrites can boost EPSP speed, particularly for small signals. Here we extend those observations and show that I_h carried mostly by HCN1, contributes to processing and transmission of auditory information in SGN cell bodies as well. Whether preservation of I_h-dependent temporal information is critical for behaviorally relevant auditory tasks such as sound localization remains to be determined.

We thank the members of the Holt/Géléoc laboratory for helpful discussions and review of previous versions of the manuscript. We thank Dr. Andreas Ludwig for kindly providing *Hcn2*-deficient mice.

This work was supported by the National Institutes of Health/National Institute on Deafness and Other Communication Disorders grant DC05439 to J.R. Holt.

Author contributions: Y.-H. Kim performed experiments, analyzed data, prepared figures, and wrote the manuscript. J.R. Holt conceived of the project, designed experiments, analyzed data, and wrote the manuscript.

Sharona E. Gordon served as editor.

Submitted: 1 May 2013
Accepted: 31 July 2013

REFERENCES

Adamson, C.L., M.A. Reid, Z.-L. Mo, J. Bowne-English, and R.L. Davis. 2002. Firing features and potassium channel content of murine spiral ganglion neurons vary with cochlear location. *J. Comp. Neurol.* 447:331–350. http://dx.doi.org/10.1002/cne.10244

Aizenman, C.D., and D.J. Linden. 1999. Regulation of the rebound depolarization and spontaneous firing patterns of deep nuclear neurons in slices of rat cerebellum. *J. Neurophysiol.* 82:1697–1709.

Altomare, C., B. Terragni, C. Brioschi, R. Milanesi, C. Pagliuca, C. Viscomi, A. Moroni, M. Baruscotti, and D. DiFrancesco. 2003. Heteromeric HCN1-HCN4 channels: a comparison with native pacemaker channels from the rabbit sinoatrial node. *J. Physiol.* 549:347–359. http://dx.doi.org/10.1113/jphysiol.2002.027698

Bakondi, G., A. Pór, I. Kovács, G. Szucs, and Z. Rusznák. 2009. Hyperpolarization-activated, cyclic nucleotide-gated, cation nonselective channel subunit expression pattern of guinea-pig spiral ganglion cells. *Neuroscience.* 158:1469–1477. http://dx.doi.org/10.1016/j.neuroscience.2008.10.056

Bal, R., and D. Oertel. 2000. Hyperpolarization-activated, mixed-cation current (I(h)) in octopus cells of the mammalian cochlear nucleus. *J. Neurophysiol.* 84:806–817.

Banks, M.I., R.A. Pearce, and P.H. Smith. 1993. Hyperpolarization-activated cation current (I_h) in neurons of the medial nucleus of the trapezoid body: voltage-clamp analysis and enhancement by norepinephrine and cAMP suggest a modulatory mechanism in the auditory brain stem. *J. Neurophysiol.* 70:1420–1432.

Biel, M., C. Wahl-Schott, S. Michalakis, and X. Zong. 2009. Hyperpolarization-activated cation channels: from genes to function. *Physiol. Rev.* 89:847–885. http://dx.doi.org/10.1152/physrev.00029.2008

BoSmith, R.E., I. Briggs, and N.C. Sturgess. 1993. Inhibitory actions of ZENECA ZD7288 on whole-cell hyperpolarization activated inward current (I_f) in guinea-pig dissociated sinoatrial node cells. *Br. J. Pharmacol.* 110:343–349. http://dx.doi.org/10.1111/j.1476-5381.1993.tb13815.x

Chen, C. 1997. Hyperpolarization-activated current (Ih) in primary auditory neurons. *Hear. Res.* 110:179–190. http://dx.doi.org/10.1016/S0378-5955(97)00078-6

Chen, W.C., H.Z. Xue, Y.L. Hsu, Q. Liu, S. Patel, and R.L. Davis. 2011. Complex distribution patterns of voltage-gated calcium channel α-subunits in the spiral ganglion. *Hear. Res.* 278:52–68. http://dx.doi.org/10.1016/j.heares.2011.01.016

Davis, R.L. 2003. Gradients of neurotrophins, ion channels, and tuning in the cochlea. *Neuroscientist.* 9:311–316. http://dx.doi.org/10.1177/1073858403251986

DiFrancesco, D. 1986. Characterization of single pacemaker channels in cardiac sino-atrial node cells. *Nature.* 324:470–473. http://dx.doi.org/10.1038/324470a0

DiFrancesco, D., and P. Tortora. 1991. Direct activation of cardiac pacemaker channels by intracellular cyclic AMP. *Nature.* 351:145–147. http://dx.doi.org/10.1038/351145a0

Echteler, S.M. 1992. Developmental segregation in the afferent projections to mammalian auditory hair cells. *Proc. Natl. Acad. Sci. USA.* 89:6324–6327. http://dx.doi.org/10.1073/pnas.89.14.6324

Felix, R.A. II, A. Fridberger, S. Leijon, A.S. Berrebi, and A.K. Magnusson. 2011. Sound rhythms are encoded by postinhibitory rebound spiking in the superior paraolivary nucleus. *J. Neurosci.* 31:12566–12578. http://dx.doi.org/10.1523/JNEUROSCI.2450-11.2011

Geisler, C.D. 1998. From Sound to Synapse: Physiology of the Mammalian Ear. Oxford University Press, New York. 381 pp.

Harris, N.C., and A. Constanti. 1995. Mechanism of block by ZD 7288 of the hyperpolarization-activated inward rectifying current in guinea pig substantia nigra neurons in vitro. *J. Neurophysiol.* 74:2366–2378.

Herrmann, S., J. Stieber, and A. Ludwig. 2007. Pathophysiology of HCN channels. *Pflugers Arch.* 454:517–522. http://dx.doi.org/10.1007/s00424-007-0224-4

Horwitz, G.C., A. Lelli, G.S. Géléoc, and J.R. Holt. 2010. HCN channels are not required for mechanotransduction in sensory hair cells of the mouse inner ear. *PLoS ONE.* 5:e8627. http://dx.doi.org/10.1371/journal.pone.0008627

Horwitz, G.C., J.R. Risner-Janiczek, S.M. Jones, and J.R. Holt. 2011. HCN channels expressed in the inner ear are necessary for normal balance function. *J. Neurosci.* 31:16814–16825. http://dx.doi.org/10.1523/JNEUROSCI.3064-11.2011

Hossain, W.A., S.D. Antic, Y. Yang, M.N. Rasband, and D.K. Morest. 2005. Where is the spike generator of the cochlear nerve? Voltage-gated sodium channels in the mouse cochlea. *J. Neurosci.* 25:6857–6868. http://dx.doi.org/10.1523/JNEUROSCI.0123-05.2005

Ishii, T.M., M. Takano, L.H. Xie, A. Noma, and H. Ohmori. 1999. Molecular characterization of the hyperpolarization-activated cation channel in rabbit heart sinoatrial node. *J. Biol. Chem.* 274:12835–12839. http://dx.doi.org/10.1074/jbc.274.18.12835

Ishii, T.M., M. Takano, and H. Ohmori. 2001. Determinants of activation kinetics in mammalian hyperpolarization-activated cation channels. *J. Physiol.* 537:93–100. http://dx.doi.org/10.1111/j.1469-7793.2001.0093k.x

Johnson, S.L., T. Eckrich, S. Kuhn, V. Zampini, C. Franz, K.M. Ranatunga, T.P. Roberts, S. Masetto, M. Knipper, C.J. Kros, and W. Marcotti. 2011. Position-dependent patterning of spontaneous action potentials in immature cochlear inner hair cells. *Nat. Neurosci.* 14:711–717. http://dx.doi.org/10.1038/nn.2803

Kane, K.L., C.M. Longo-Guess, L.H. Gagnon, D. Ding, R.J. Salvi, and K.R. Johnson. 2012. Genetic background effects on age-related hearing loss associated with *Cdh23* variants in mice. *Hear. Res.* 283:80–88. http://dx.doi.org/10.1016/j.heares.2011.11.007

Koch, U., and B. Grothe. 2003. Hyperpolarization-activated current (Ih) in the inferior colliculus: distribution and contribution to temporal processing. *J. Neurophysiol.* 90:3679–3687. http://dx.doi.org/10.1152/jn.00375.2003

Kopp-Scheinpflug, C., A.J.B. Tozer, S.W. Robinson, B.L. Tempel, M.H. Hennig, and I.D. Forsythe. 2011. The sound of silence: ionic mechanisms encoding sound termination. *Neuron.* 71:911–925. http://dx.doi.org/10.1016/j.neuron.2011.06.028

Kros, C.J., J.P. Ruppersberg, and A. Rüsch. 1998. Expression of a potassium current in inner hair cells during development of hearing in mice. *Nature.* 394:281–284. http://dx.doi.org/10.1038/28401

Leao, R.N., H. Sun, K. Svahn, A. Berntson, M. Youssoufian, A.G. Paolini, R.E.W. Fyffe, and B. Walmsley. 2006. Topographic organization in the auditory brainstem of juvenile mice is disrupted in congenital deafness. *J. Physiol.* 571:563–578. http://dx.doi.org/10.1113/jphysiol.2005.098780

Lelli, A., Y. Asai, A. Forge, J.R. Holt, and G.S. Géléoc. 2009. Tonotopic gradient in the developmental acquisition of sensory transduction in outer hair cells of the mouse cochlea. *J. Neurophysiol.* 101:2961–2973. http://dx.doi.org/10.1152/jn.00136.2009

Liberman, M.C. 1982. Single-neuron labeling in the cat auditory nerve. *Science.* 216:1239–1241. http://dx.doi.org/10.1126/science.7079757

Lu, C.C., J.M. Appler, E.A. Houseman, and L.V. Goodrich. 2011. Developmental profiling of spiral ganglion neurons reveals insights into auditory circuit assembly. *J. Neurosci.* 31:10903–10918. http://dx.doi.org/10.1523/JNEUROSCI.2358-11.2011

Ludwig, A., X. Zong, M. Jeglitsch, F. Hofmann, and M. Biel. 1998. A family of hyperpolarization-activated mammalian cation channels. *Nature.* 393:587–591. http://dx.doi.org/10.1038/31255

Ludwig, A., X. Zong, J. Stieber, R. Hullin, F. Hofmann, and M. Biel. 1999. Two pacemaker channels from human heart with profoundly different activation kinetics. *EMBO J.* 18:2323–2329. http://dx.doi.org/10.1093/emboj/18.9.2323

Ludwig, A., T. Budde, J. Stieber, S. Moosmang, C. Wahl, K. Holthoff, A. Langebartels, C. Wotjak, T. Munsch, X. Zong, et al. 2003. Absence epilepsy and sinus dysrhythmia in mice lacking the pacemaker channel HCN2. *EMBO J.* 22:216–224. http://dx.doi.org/10.1093/emboj/cdg032

Lüthi, A., and D.A. McCormick. 1998. Periodicity of thalamic synchronized oscillations: the role of Ca^{2+}-mediated upregulation of I_h. *Neuron.* 20:553–563. http://dx.doi.org/10.1016/S0896-6273(00)80994-0

Lv, P., D. Wei, and E.N. Yamoah. 2010. Kv7-type channel currents in spiral ganglion neurons: involvement in sensorineural hearing loss. *J. Biol. Chem.* 285:34699–34707. http://dx.doi.org/10.1074/jbc.M110.136192

Lv, P., C.-R. Sihn, W. Wang, H. Shen, H.J. Kim, S.M. Rocha-Sanchez, and E.N. Yamoah. 2012. Posthearing $Ca^{(2+)}$ currents and their roles in shaping the different modes of firing of spiral ganglion neurons. *J. Neurosci.* 32:16314–16330. http://dx.doi.org/10.1523/JNEUROSCI.2097-12.2012

Meyer, A.C., and T. Moser. 2010. Structure and function of cochlear afferent innervation. *Curr. Opin. Otolaryngol. Head Neck Surg.* 18:441–446. http://dx.doi.org/10.1097/MOO.0b013e32833e0586

Mo, Z.-L., and R.L. Davis. 1997. Heterogeneous voltage dependence of inward rectifier currents in spiral ganglion neurons. *J. Neurophysiol.* 78:3019–3027.

Moosmang, S., M. Biel, F. Hofmann, and A. Ludwig. 1999. Differential distribution of four hyperpolarization-activated cation channels in mouse brain. *Biol. Chem.* 380:975–980. http://dx.doi.org/10.1515/BC.1999.121

Nagtegaal, A.P., and J.G. Borst. 2010. In vivo dynamic clamp study of I(h) in the mouse inferior colliculus. *J. Neurophysiol.* 104:940–948. http://dx.doi.org/10.1152/jn.00264.2010

Nolan, M.F., G. Malleret, K.H. Lee, E. Gibbs, J.T. Dudman, B. Santoro, D. Yin, R.F. Thompson, S.A. Siegelbaum, E.R. Kandel, and A. Morozov. 2003. The hyperpolarization-activated HCN1 channel is important for motor learning and neuronal integration by cerebellar Purkinje cells. *Cell.* 115:551–564. http://dx.doi.org/10.1016/S0092-8674(03)00884-5

Nolan, M.F., G. Malleret, J.T. Dudman, D.L. Buhl, B. Santoro, E. Gibbs, S. Vronskaya, G. Buzsáki, S.A. Siegelbaum, E.R. Kandel, and A. Morozov. 2004. A behavioral role for dendritic integration: HCN1 channels constrain spatial memory and plasticity at inputs to distal dendrites of CA1 pyramidal neurons. *Cell.* 119:719–732.

Perkins, R.E., and D.K. Morest. 1975. A study of cochlear innervation patterns in cats and rats with the Golgi method and Nomarski optics. *J. Comp. Neurol.* 163:129–158. http://dx.doi.org/10.1002/cne.901630202

Pujol, R., M. Lavigne-Rebillard, and M. Lenoir. 1998. Development of sensory and neural structures in the mammalian cochlea. *In* Development of the Auditory System. E.W. Rubel, A.N. Popper, and R.R. Fay, editors. Springer-Verlag, New York. 146–192.

Robinson, R.B., and S.A. Siegelbaum. 2003. Hyperpolarization-activated cation currents: from molecules to physiological function. *Annu. Rev. Physiol.* 65:453–480. http://dx.doi.org/10.1146/annurev.physiol.65.092101.142734

Romand, M.R., and R. Romand. 1987. The ultrastructure of spiral ganglion cells in the mouse. *Acta Otolaryngol.* 104:29–39. http://dx.doi.org/10.3109/00016488709109044

Romand, R. 1983. Development of the cochlea. *In* Development of Auditory and Vestibular Systems. R. Romand editor. Academic Press, New York. 47–88.

Rubel, E.W., and B. Fritzsch. 2002. Auditory system development: primary auditory neurons and their targets. *Annu. Rev. Neurosci.* 25:51–101. http://dx.doi.org/10.1146/annurev.neuro.25.112701.142849

Rusznák, Z., and G. Szűcs. 2009. Spiral ganglion neurones: an overview of morphology, firing behaviour, ionic channels and function. *Pflugers Arch.* 457:1303–1325. http://dx.doi.org/10.1007/s00424-008-0586-2

Santoro, B., S. Chen, A. Lüthi, P. Pavlidis, G.P. Shumyatsky, G.R. Tibbs, and S.A. Siegelbaum. 2000. Molecular and functional heterogeneity of hyperpolarization-activated pacemaker channels in the mouse CNS. *J. Neurosci.* 20:5264–5275.

Santos-Sacchi, J. 1993. Voltage-dependent ionic conductances of type I spiral ganglion cells from the guinea pig inner ear. *J. Neurosci.* 13:3599–3611.

Simmons, D.D., L. Manson-Gieseke, T.W. Hendrix, K. Morris, and S.J. Williams. 1991. Postnatal maturation of spiral ganglion neurons: a horseradish peroxidase study. *Hear. Res.* 55:81–91. http://dx.doi.org/10.1016/0378-5955(91)90094-P

Stieber, J., S. Herrmann, S. Feil, J. Löster, R. Feil, M. Biel, F. Hofmann, and A. Ludwig. 2003. The hyperpolarization-activated channel HCN4 is required for the generation of pacemaker action potentials in the embryonic heart. *Proc. Natl. Acad. Sci. USA.* 100:15235–15240. http://dx.doi.org/10.1073/pnas.2434235100

Szabó, Z.S., C.S. Harasztosi, I. Sziklai, G. Szûcs, and Z. Rusznák. 2002. Ionic currents determining the membrane characteristics of type I spiral ganglion neurons of the guinea pig. *Eur. J. Neurosci.* 16:1887–1895. http://dx.doi.org/10.1046/j.1460-9568.2002.02258.x

Taberner, A.M., and M.C. Liberman. 2005. Response properties of single auditory nerve fibers in the mouse. *J. Neurophysiol.* 93:557–569. http://dx.doi.org/10.1152/jn.00574.2004

Tritsch, N.X., and D.E. Bergles. 2010. Developmental regulation of spontaneous activity in the Mammalian cochlea. *J. Neurosci.* 30:1539–1550. http://dx.doi.org/10.1523/JNEUROSCI.3875-09.2010

Tritsch, N.X., E. Yi, J.E. Gale, E. Glowatzki, and D.E. Bergles. 2007. The origin of spontaneous activity in the developing auditory system. *Nature.* 450:50–55. http://dx.doi.org/10.1038/nature06233

Yamada, R., H. Kuba, T.M. Ishii, and H. Ohmori. 2005. Hyperpolarization-activated cyclic nucleotide-gated cation channels regulate auditory coincidence detection in nucleus laminaris of the chick. *J. Neurosci.* 25:8867–8877. http://dx.doi.org/10.1523/JNEUROSCI.2541-05.2005

Yi, E., I. Roux, and E. Glowatzki. 2010. Dendritic HCN channels shape excitatory postsynaptic potentials at the inner hair cell afferent synapse in the mammalian cochlea. *J. Neurophysiol.* 103:2532–2543. http://dx.doi.org/10.1152/jn.00506.2009

Zheng, Q.Y., K.R. Johnson, and L.C. Erway. 1999. Assessment of hearing in 80 inbred strains of mice by ABR threshold analyses. *Hear. Res.* 130:94–107. http://dx.doi.org/10.1016/S0378-5955(99)00003-9